Tuning Co-Cu-Al catalysts and their reaction conditions on the CO2 hydrogenation reaction to higher alcohols under mild conditions

Vitor Duarte Lage, Anthony Le Valant, Nicolas Bion, Fabio Souza Toniolo

Tuning Co-Cu-Al catalysts and their reaction conditions on the CO_2 hydrogenation reaction to higher alcohols under mild conditions.

Vitor Duarte Lage[a], Anthony Le Valant[b], Nicolas Bion[b], Fabio Souza Toniolo[a]

[a] *Chemical Engineering Program – PEQ/COPPE – Universidade Federal do Rio de Janeiro, Cidade Universitária, Rio de Janeiro CEP 21941-972, RJ, Brazil*

[b] *Institut de Chimie des Milieux et Matériaux de Poitiers (IC2MP)/Université de Poitiers - CNRS, Poitiers, France*

Abstract

The catalytic conversion of CO_2 and H_2 into valuable chemicals is a promising alternative to the recent energy and environmental challenges. However, designing an earth-abundant catalyst capable of actively and selectively converting CO_2 into desirable products is yet a challenge. Herein, we report on a facile K-Co-Cu-Al catalyst prepared by a coprecipitation method for CO_2 hydrogenation to higher alcohols (HAs). We investigated different Co:Cu ratios, reduction temperatures, and reaction conditions (temperature, space velocity, and H_2/CO_2 ratio) to tune it, enhancing the selectivity and yield of higher alcohols. $Co_{1.8}Cu_{0.9}AlO_x$ (1 wt% K), reduced at 400 ºC, exhibits a high HAs selectivity of 44.8% (20.8% for ethanol) and space-time yield of 5.54 $mmol \cdot h^{-1} \cdot g_{cat}^{-1}$ (3.08 $mmol \cdot h^{-1} \cdot g_{cat}^{-1}$ of ethanol), under mild conditions (250 ºC, 30 bar, H_2/CO_2 ratio of 1.5, and 14200 $mL \cdot g_{cat}^{-1} \cdot h^{-1}$), which represents one of the best performances among related studies, especially among Co-based catalysts.

Keywords: CO_2 hydrogenation; Ethanol production; CO_2 conversion; Co-based catalyst; Cu-based catalyst; Bimetallic catalyst.

Graphical Abstract

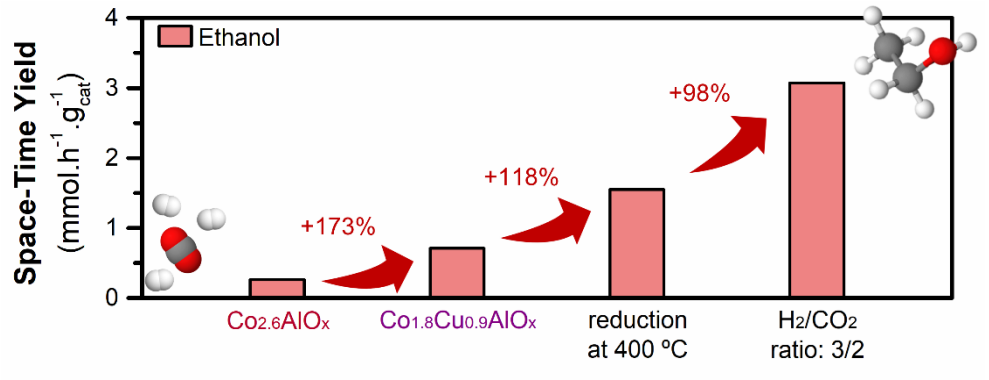

1. Introduction

One of the most significant current scientific challenges is reducing the atmospheric concentration of CO_2, an anthropogenic greenhouse gas responsible for global warming. To address this challenge three main strategies can be employed: (i) reducing emissions; (ii) capturing and storing; and (iii) utilizing or transforming CO_2. In that sense, the CO_2 hydrogenation reaction emerges as a promising alternative to both capture and transform this anthropogenic gas, as CO_2, captured from industrial effluents, can serve as a C1 building block to produce value-added products and feedstock [1,2]. However, the CO_2 hydrogenation reaction can yield various possible products, including CO, CH_4, C_{2+} hydrocarbons (HCs), methanol, and higher alcohols (HAs or $C_{2+}OH$), each with its advantages, disadvantages, and academic challenges [3–6].

Among these products, higher alcohols, particularly ethanol, have garnered significant research and industrial attention due to their versatile applications as fuel, solvents, chemical precursors, and cleaning agents. They also offer higher energy density, sustainability, and reduced environmental impact compared to alternative substances [3,5–8]. Nonetheless, tailoring the catalysts, and optimizing the process condition are key challenges in this field [4,5].

For the synthesis of HAs via CO_2 hydrogenation, various catalysts have been reported [9–16], but certain trends have been identified, including Rh-based, Cu-based, Co-based [5,6,8], Pd-based [5], and Mo-based [6,8] catalysts. Among these, Co- and Cu-based catalysts stand out as non-noble metal catalysts [11], offering relative cost advantages. Co-based catalysts exhibit higher CO_2 conversion [5,6,8], but methane is typically the predominant product formed [11], particularly in

their metallic form (Co^0). However, recent studies have demonstrated that modifying Co-based catalysts through alloy formation or interaction with some oxide supports can reduce their ability to break the C-O bond, favoring HAs formation [5,8]. These modified Co-based catalysts ($CoAlO_x$, Na-Co/SiO_2, Pt/Co_3O_4, $LaCoGaO_3$, $CoNiAlO_x$) have been studied in both continuous and batch reactions for HAs synthesis, exhibiting CO_2 conversion ranging from 5-67%, selectivity to HAs from 0.05-92%, and space-time yield (STY) from 0.01-2.16 $mmol \cdot h^{-1} \cdot g_{cat}^{-1}$ [8].

Cu has emerged as a promising metal for Co-based alloys [14,17], as it promotes CO-insertion [18] and inhibits C-O bond cleavage [8,19]. Additionally, alkali metals have been investigated as promoters to enhance basicity by donating electrons to Co sites. Amidst, Na, and K have been extensively studied for HAs synthesis, as they have been reported to reduce CH_4 formation, increase CO_2 conversion, and tune HAs selectivity [5,6,11,20,21]. However, excess Na (>5 wt%) can inhibit CO insertion, increasing CO selectivity [8]. For K, a wide range of weight content (0.1-17.6 wt%) has been explored, with optimal composition falling between 0.5 to 4.6 wt% [11,12,20–23].

Regarding the reaction conditions, determining the optimal temperature, H_2/CO_2 ratio, and space velocity, among other parameters, is detrimental to improving the HAs synthesis. Temperature plays a dual role, favoring CO_2 conversion with its increase but hindering HAs formation [5,24]. Similarly, increasing the H_2/CO_2 ratio also favors conversion, but excess H_2 can further hydrogenate the reaction intermediate of ethanol, while decreasing it can favor methanol synthesis routes [5,25]. Adjusting the space velocity (SV) is also vital. Increasing SV results in lower conversion, whereas lower velocities can favor some reaction pathways over others, leading to undesired products [5,9,26]. In summary, optimizing these conditions is necessary to strike a balance between conversion and product selectivity, thereby increasing the yield of the desired product [5]. Most Co-based catalysts exhibit optimal performance in the temperature range of 140-250 ºC with space velocity between 3000-6000 $mL \cdot h^{-1} \cdot g_{cat}^{-1}$ [6]. However, the effect of the H_2/CO_2 ratio has not been widely explored.

To address the need for improving CO_2 conversion and inhibiting the formation of undesired products, mainly methane, we propose investigating CoCu catalysts. In this study, we prepared a

series of $Co_{(2.8-n)}Cu_nAlO_x$ catalysts derived from layered-double hydroxides (LDH), carefully tailored to retain 1 wt% of K. LDHs have garnered attention as promising precursors for heterogeneous catalysts due to their thermal stability and the possibility of modifying the characteristics of the resulting material such as surface area, particle size, electronic state and distribution of metal species [14,27,28]. Moreover, LDH-derived catalysts can easily be synthesized on a large scale via coprecipitation and have shown promising results in CO_2 hydrogenation to ethanol [11,14,24,29].

Herein, we aim to explore different Co:Cu ratios, reduction temperatures, and reaction conditions (temperature, space velocity, and H_2/CO_2 ratio) to investigate their effects on CO_2 conversion, product selectivity, and yield. By fine-tuning the catalyst design and optimizing the reaction conditions, we aspire to overcome the thermodynamic and kinetic limitations associated with CO2 hydrogenation and enhance the efficiency and viability of higher alcohol synthesis.

2. Experimental

2.1 Catalyst Preparation

The $Co_{(2.8-n)}Cu_nAlO_x$ samples were derived from the calcination of LDH clays, which were prepared by a modified coprecipitation method [30,31]. The alkaline solution was formed by 2 M NaOH (Sigma-Aldrich, ≥98%) and 0.5 M Na_2CO_3 (Sigma-Aldrich, ≥99.5%). The precursor solution (1 M) was prepared by dissolving $Co(NO_3)_2{\cdot}6H_2O$ (Sigma-Aldrich, ≥98%), $Cu(NO_3)_2{\cdot}2.5H_2O$ (Sigma-Aldrich, ≥98%), and $Al(NO_3)_3{\cdot}9H_2O$ (Sigma-Aldrich, ≥98%), in deionized water, with the desired Co:Cu:Al molar ratio. The chosen M:Al ratio (M: active metals, i.e., Co and Cu) was 2.8, based on other works reporting similar materials [30–34]. The selected molar ratios of Co and Cu, expressed by the Co/(Co+Cu), were 0, 0.5, 0.66, and 1.

Both the precursor and alkaline solutions were added drop-wise to a recipient under agitation, maintaining pH 10 by regulating the flow of the alkaline solution. After adding the precursor solution, the resulting solution was aged overnight, filtered, and washed thoroughly in deionized water to remove excess sodium [30,31]. The resulting filtered cake was suspended in a K_2CO_3 with concentration adjusted to obtain approximately 1 wt% K in the catalyst [34,35]. Finally, the resulting sludge was filtered and calcined in a muffle furnace in static air at 500 ºC for 3 h [34,36].

2.2 Characterization

The metal content in each prepared sample was determined by ICP-OES (Inductively Coupled Plasma Optical Emission Spectrometry) on a Perkin Elmer Optima 2000DV spectrometer. Prior to analysis, the samples underwent acid digestion, i.e., dissolved in an HNO_3/HCl acidic mixture (1:3 ratio) and heated by microwave. The solution was then injected into the plasma as an aerosol generated by a nebulizer.

The identification of the crystalline phases and crystallographic properties of the prepared samples were analyzed via X-ray diffraction (XRD) collected on a Rigaku Miniflex diffractometer (30 kV, and 15 mA) with an X-ray tube Cu target (CuKα, λ=1,5418 Å). The diffractograms were collected with Bragg angles ranging from 10º to 80º, using a continuous scan mode with a step size of 0.05º and a collection time of 1 s per step.

The textural properties such as surface area (A_{BET}), pore volume (V_{pore}), and pore diameter (d_{pore}) of the calcined catalysts were determined by N_2 physisorption using a Micromeritics Tristar instrument and calculated according to the method of Brunauer, Emmet and Teller (BET). The samples were degassed at 200 ºC overnight before the N_2 physisorption analysis.

The reduction profile of the catalysts was analyzed in temperature-programmed reduction (TPR) experiments employing a Micromeritics Autochem II 2920 apparatus equipped with a thermal conductivity detector (TCD). The samples were pretreated at 200 ºC with an Ar flow (30 mL·min^{-1}) for 1 h. Subsequently, the TPR experiments were carried out with approximately 125 mg of catalyst in a 10% H_2/Ar flow (30 mL·min^{-1}) from 30 to 1000 ºC (5 ºC·min^{-1}) using a programmable temperature controller. The reduction degree was then calculated by dividing the real H_2-intake by the theoretical H_2-intake, which, was determined based on the ICP-OES results.

The basicity profile of the catalysts was analyzed in CO_2 temperature-programmed desorption (CO_2-TPD) experiments in a multipurpose testing unit equipped with an online quadrupole mass detector QUADSTAR 422 (QMS 200, BALZERS). For that, the sample (100 mg) was placed into a quartz tube reactor, which was heated (10 ºC·min^{-1}) to the desired temperatures (250, 400, and 500 ºC) under pure H_2 flow (60 mL·min^{-1}) for 30 min, and then cooled to room temperature in ultra-high purity He flow (60 mL·min^{-1}). After pretreatment, the CO_2 adsorption stage was conducted

by passing pure CO_2 (30 mL·min^{-1}) for 30 min and then flushing the reaction with He (60 mL·min^{-1}) for 60 min. The TPD was performed by heating (20 ºC·min^{-1}) the sample to 800 ºC. The effluent gases were monitored by an online mass detector (m/z = 2, 4, 28, 30, 32, 44, and 46).

2.3 Catalytic Test

The CO_2 hydrogenation catalytic tests for the $Co_{(2.8-n)}Cu_nAlO_x$ samples were executed in a continuous fixed-bed stainless steel reactor. The sample (300 mg, 0.160-0.100 mm sieved fraction) was placed between two layers of SiC (0.125 mm), enough to ensure an 8 cm height reaction bed and to maintain the fluid dynamic conditions between different samples. Prior to the reaction, the samples underwent *in situ* reduction at four different temperatures (250, 300, 400, and 500 ºC) for 30 min (heating ramp: 5 ºC.min^{-1}) under pure H_2 flow (30 ml·min^{-1}).

The initial tests were conducted at 250 ºC and 30 bar in an $H_2/CO_2/N_2$ flow (ratio: 3/1/0.25) with gas-hourly space velocity (GHSV) set to 14200 mL·g_{cat}^{-1}·h^{-1} for 24 h. Subsequently, different H_2/CO_2 ratio ($H_2/CO_2/N_2$ ratio: 3/2/0.25), GHSV (10625 mL.g_{cat}^{-1}.h^{-1}) and temperatures (200, 250 and 300 ºC) were explored. The outlet products were analyzed online (each 36 min) in an Agilent 7890A gas chromatograph (GC). The gas products (CO, CO_2, H_2, and N_2) were detected by a TCD detector. Hydrocarbons and condensable liquid products were analyzed by an FID detector. The catalytic performance was expressed by CO_2 conversion (X_{CO_2}), C-based product selectivity (S_i), and the product space-time yield (STY_i), calculated by the equation as follows:

$$X_{CO_2} = \frac{[CO_2]_{in} - [CO_2]_{out}}{[CO_2]_{in}} \times 100\% \quad (1)$$

$$S_i = \frac{n_i \times C_i}{\sum(n_i \times C_i)} \times 100\% \quad (2)$$

$$STY_i = \frac{F_{CO_2,in} \times X_{CO_2} \times S_i}{m_{cat}} \quad (3)$$

where $[CO_2]_{in}$ and $[CO_2]_{out}$, respectively, are the molar concentration of CO_2 in the inlet and outlet flow; Ci refers the concentration of products (CO, CH_4, C_xH_n, CH_3OH, C_2H_5OH, C_3H_7OH, among others) in the outlet flow; n_i represents the number of carbon atoms for product C_i; $F_{CO2,in}$ stands for the flow rate of CO_2; and m_{cat} is the mass of catalyst.

3. Results and Discussion

3.1 Physical-Chemical Properties

The metallic weight content (wt%) obtained for the samples on the ICP-OES analysis, the calculated molar ratio between Co:Cu:Al, and their textural properties, are summarized in **Table 1**. Henceforth the catalysts are referred to as $Cu_{2.6}AlO_x$, $Co_{1.3}Cu_{1.3}AlO_x$, $Co_{1.8}Cu_{0.9}AlO_x$, and $Co_{2.6}AlO_x$, according to their Co:Cu:Al ratios. We verified that the Co/(Co+Cu) ratios agreed with expected nominal values and that obtaining an M-Al ratio close to 2.8 was possible, as desired. The samples did not present any detectable amounts of Na, confirming that the treatment with K_2CO_3 solution was efficiently removed the excess Na. The K content for $Cu_{2.6}AlO_x$, $Co_{1.3}Cu_{1.3}AlO_x$, $Co_{1.8}Cu_{0.9}AlO_x$, and $Co_{2.6}AlO_x$ was 0.8, 0.7, 0.8 and 0.9 wt%, respectively, close to the expected 1 wt%.

Table 1. Content of Co, Cu, Al, and K (determined by ICP-OES), Surface area (A_{BET}), pore volume (V_{pore}), and pore diameter (d_{pore}) of the prepared catalysts after calcination at 500 ºC.

Catalyst	Metallic content (wt%)				Co:Cu:Al	A_{BET}	V_{pore}	d_{pore}
	Al	Co	Cu	K	Ratio	($m^2 \cdot g^{-1}$)	($cm^3 \cdot g^{-1}$)	(nm)
$Cu_{2.6}AlO_x$	9.3	0.0	57.5	0.8	0:2.6:1	56	0.18	9
$Co_{1.3}Cu_{1.3}AlO_x$	9.3	27.3	29.3	0.7	1.3:1.3:1	85	0.44	19
$Co_{1.8}Cu_{0.9}AlO_x$	9.0	34.9	18.7	0.8	1.8:0.9:1	69	0.37	18
$Co_{2.6}AlO_x$	9.1	52.2	0.0	0.9	2.6:0:1	78	0.35	13

Regarding the N_2 physisorption isotherms for $Cu_{2.6}AlO_x$ (blue), $Co_{1.3}Cu_{1.3}AlO_x$ (light purple), $Co_{1.8}Cu_{0.9}AlO_x$ (dark purple), and $Co_{2.6}AlO_x$ (red) are shown in **Figure 1**. Based on the N_2 physisorption analysis, the calculated BET surface area for $Cu_{2.6}AlO_x$, $Co_{1.3}Cu_{1.3}AlO_x$, $Co_{1.8}Cu_{0.9}AlO_x$, and $Co_{2.6}AlO_x$. was 56, 85, 69, and 78 $m^2 \cdot g^{-1}$, in that order. The values agree with the expected area (50-150 $m^2 \cdot g^{-1}$) for mixed oxides prepared by the modified coprecipitation method [30,36]. Moreover, the hysteresis at high relative pressure (**Figure 1**) indicates the formation of a mesoporous material

[37], which is consistent with similar previously reported materials [27,32,37–39] and with the values of pore diameter (**Table 1**).

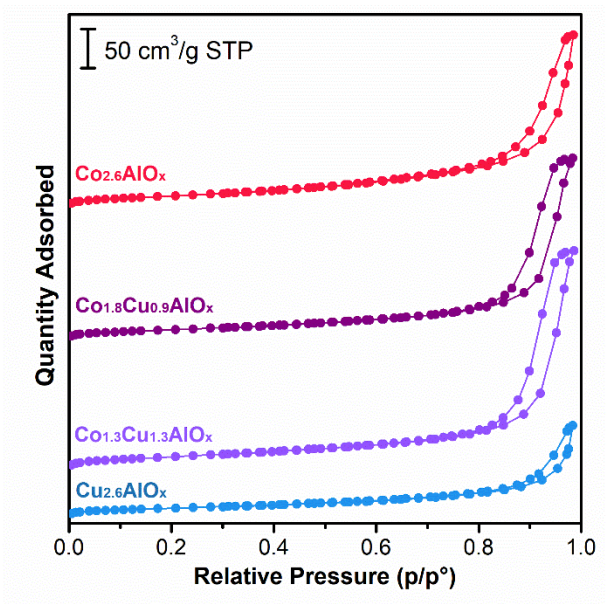

Figure 1. Nitrogen adsorption isotherms of for $Cu_{2.6}AlO_x$ (blue), $Co_{1.3}Cu_{1.3}AlO_x$ (light purple), $Co_{1.8}Cu_{0.9}AlO_x$ (dark purple), and $Co_{2.6}AlO_x$ (red).

Powder XRD patterns for the samples calcined at 500 ºC are presented in **Figure 2**. For $Cu_{2.6}AlO_x$ (blue), a CuO (tenorite, PDF#48-1548) phase was identified. It is also possible to infer the presence of small and poorly defined peaks that could be attributed to $CuAl_2O_4$ spinel (PDF#44-0106). For $Co_{2.6}AlO_x$ (red), the Co_3O_4 (PDF#43-1003) and the Co_2AlO_4 inverse spinel (PDF#38-0814) phases were compatible with the XRD pattern. It is also possible to infer the presence of $CoAl_2O_4$ spinel (PDF#44-0106), as it presents the same position of diffraction lines only slightly shifted to a lower angle. From the XRD patterns, it is difficult to distinguish Co_3O_4 from spinel-like structures, as their lattice parameters are very similar [39]. As for $Co_{1.3}Cu_{1.3}AlO_x$ (light purple) and $Co_{1.8}Cu_{0.9}AlO_x$ (dark purple), the presence of a mix of CuO, Co_3O_4, and the Co-Al spinel-like structures is the likely case. It is also reported on Co-Cu mixed oxides, such as $Co_{2.2}Cu_{0.8}O_4$ (PDF#36-1189), $Co_{2.05}Cu_{0.95}O_4$ (PDF#36-1189), and $Co_{2.84}Cu_{0.15}O_4$ (PDF#36-1189), to display the same diffraction pattern as Co_3O_4, with a slight shift in angle due to the small difference in Co and Cu cationic radii, which implies that, through XRD, it is difficult to determine whether the pattern

corresponds to Co_3O_4 or a Co-Cu spinel [32,40]. Recent works reported similar materials containing a mixture of different phases and spinel structures [31–33,37,39].

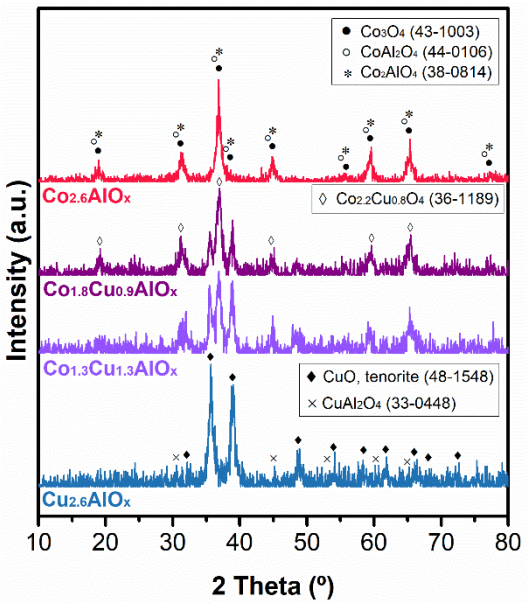

Figure 2. $Cu_{2.6}AlO_x$ (blue), $Co_{1.3}Cu_{1.3}AlO_x$ (light purple), $Co_{1.8}Cu_{0.9}AlO_x$ (dark purple), and $Co_{2.6}AlO_x$ (red) XRD patterns (CuKα, λ=1,5418 Å).

The reduction profiles of the samples calcined at 500 ºC were obtained using H_2-TPR and are presented in **Figure 3**. For $Cu_{2.6}AlO_x$ (blue), we observed a single reduction region around 200 and 300 ºC, marking the reduction of Cu^{2+} to Cu^0 [41]. Similar reduction profiles for Cu-Al catalysts derived from LDHs are reported in the literature [38,42–44]. For $Co_{2.6}AlO_x$ (red), we can ascribe at least three distinct reduction regions: a peak at 250 ºC, a broad region from 350 to 450 ºC, and a broad peak around 700 ºC. The first peak and region are commonly attributed to the reduction of Co^{3+} to Co^{2+}, and the reduction of Co^{2+} to Co^0, whereas reduction peaks above 450 ºC were previously attributed to the reduction of spinel-like structures [27,35,45]. Furthermore, Co-Al catalysts derived from LDHs have been reported with two distinct reduction regions, one around 250-450 ºC, attributed to the reduction of Co^{3+} to Co^{2+}, and other one around 550-700 ºC, assigned to the reduction of Co^{2+} to Co^0 [24,45–48]. For $Co_{1.3}Cu_{1.3}AlO_x$ (light purple) and $Co_{1.8}Cu_{0.9}AlO_x$ (dark purple), we observed two distinct regions: one from 200 to 400 ºC, which could be attributed to, first, the reduction of Cu^{2+} to Cu^0, along with the reduction of Co^{3+} to Co^{2+} [31,32,37].; and a second broad

region above 400 ºC, ascribed to the two-step reduction of bulk Co^{3+} to Co^0, the reduction of Co^{2+} to Co^0, and the reduction of spinel-like structures [31,37]. It is worth mentioning that adding Cu to the Co-Al structure significantly reduced its reduction temperature. Moreover, when compared, $Co_{1.3}Cu_{1.3}AlO_x$ and $Co_{1.8}Cu_{0.9}AlO_x$, the reduction profile of $Co_{1.3}Cu_{1.3}AlO_x$ is slightly shifted to a lower temperature. This shift to lower reduction temperatures of Co-containing catalysts can be explained by hydrogen spillover from Cu metallic particles [31,32,37,49,50].

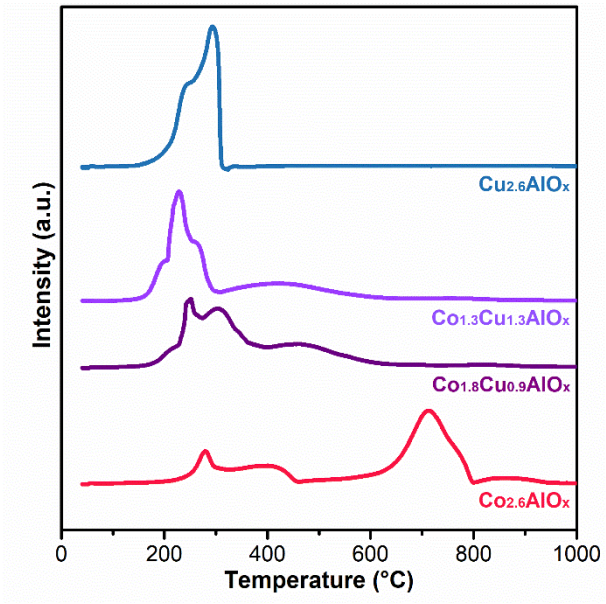

Figure 3. H_2 TPR profile of $Cu_{2.6}AlO_x$ (blue), $Co_{1.3}Cu_{1.3}AlO_x$ (dark purple), $Co_{1.8}Cu_{0.9}AlO_x$ (dark purple), and $Co_{2.6}AlO_x$ (red) under 10% H_2 flow (30 $mL.min^{-1}$).

Based on the TPR analysis and elemental analysis of Co and Cu, we calculated the degree of reduction of the samples. It is expressed as the experimental H_2 consumption (based on the peak area of the TPR profiles) divided by the theoretical H_2 consumption (based on the nominal molar content of Co and Cu in the samples, considering all Co as Co_3O_4, and all Cu as CuO) in percentage. That information is summarized in **Table 2**. The degree of reduction ranged from 88% to 99% with the increase in Cu content in the samples. In other words, the measured H_2 consumption was lower than the expected H_2 consumption, which could mean that not all Co is present as Co_3O_4, mostly likely due to spinel-like structures.

Table 2. Calculated experimental and theoretical H_2 consumption, and degree of reduction based on the 10% H_2-TPR profiles of the catalysts.

Catalyst	Experimental H_2 consumption ($mmol \cdot g^{-1}$)	Theoretical H_2 consumption ($mmol \cdot g^{-1}$)	Degree of Reduction (%)
$Cu_{2.6}AlO_x$	8.97	9.05	99
$Co_{1.3}Cu_{1.3}AlO_x$	9.62	10.79	89
$Co_{1.8}Cu_{0.9}AlO_x$	9.70	10.84	89
$Co_{2.6}AlO_x$	10.44	11.81	88

Information regarding surface basicity, an essential aspect of CO_2 hydrogenation catalysts, was assessed through CO_2-TPD experiments for the catalysts and is shown in **Figure 4**. All samples reduced at 250 ºC (**Figure 4a**) displayed a sharp peak around 110 ºC and a sinusoidal pattern from 150 to 350 ºC due to the re-adsorption of CO_2[51–54] $Co_{1.3}Cu_{1.3}AlO_x$ and $Co_{1.8}Cu_{0.9}AlO_x$ also displayed a broader peak around 250 and 300 ºC. That broad peak at intermediate temperature became prominent when $Co_{1.8}Cu_{0.9}AlO_x$ was reduced at 400 ºC, but it disappeared when it was reduced at 500 ºC (**Figure 4c**). Contrastingly, $Co_{2.6}AlO_x$, after reduction at 500 ºC, displayed a sharp at 200 ºC and a tail indicating CO_2 desorption up until 700 ºC (**Figure 4b**). It is worth mentioning that CO_2-TPD experiments were carried out at different reduction temperatures for $Co_{2.6}AlO_x$ and $Co_{1.8}Cu_{0.9}AlO_x$, as these samples were tested in such conditions in the CO_2 hydrogenation reaction (section 3.2.2).

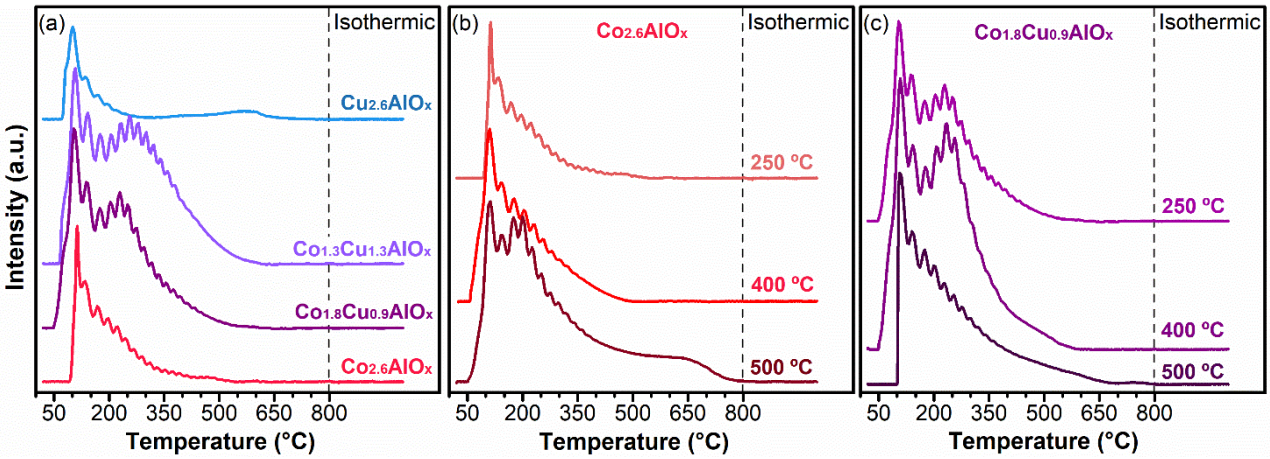

Figure 4. CO_2-TPD curves for the catalysts reduced at 250 ºC (a), and for $Co_{2.6}AlO_x$ (b), $Co_{1.8}Cu_{0.9}AlO_x$ (c), after different reduction temperatures.

According to the literature, it is possible to divide the CO_2-TPD profile into three regions according to the strength of the adsorption site. Below 200 ºC, the desorption is ascribed to weakly adsorbed CO_2 [15–17,55–57]. This region can be assigned to Bronsted basicity sites, i.e., surface hydroxyl (-OH) [15,58–60]. The second desorption region, from 200 to 500 ºC, is attributed to moderately adsorbed CO_2 [15,16,55,60] and associated with Lewis basicity, ergo oxygen sites [59], more specifically metal-oxygen pairs (M-O) [60]. It is reported that these moderate basic sites contribute to ethanol formation [25] and the activity of catalysts on the CO_2 hydrogenation reaction at that range of temperature [15]. The last region, above 500 ºC, is attributed to strong basic sites [17,55], also associated with Lewis basicity [59], more specifically to low coordination oxygen atoms [60]. Strong CO_2 adsorption sites are reported to favor CO_2 methanation [61] and, in the case of Co-based catalysts, are associated with Co^0 species [17].

Therefore, it is possible to infer that combining Co and Cu led to an increase in CO_2 adsorption, which becomes evident when comparing the calculated CO_2 uptake from the monometallic catalysts, $Cu_{2.6}AlO_x$ and $Co_{2.6}AlO_x$, to the bimetallic catalysts, $Co_{1.3}Cu_{1.3}AlO_x$ and $Co_{1.8}Cu_{0.9}AlO_x$, which is summarized in **Table 3**. $Co_{1.3}Cu_{1.3}AlO_x$ and $Co_{1.8}Cu_{0.9}AlO_x$ (**Figure 4a**) also displayed a desorption peak at the moderate basicity region (250 ºC), attributed to CO_2 hydrogenation activity. Furthermore, the moderate basicity peak on the TPD profile of $Co_{1.8}Cu_{0.9}AlO_x$ increased when the sample was reduced at 400 ºC (**Figure 4c**), leading to nearly double CO_2 uptake. Upon reducing $Co_{1.8}Cu_{0.9}AlO_x$ at 500 ºC, the CO_2 uptake was cut to half, and the peak at

250 ºC disappeared. The CO_2 uptake of $Co_{2.6}AlO_x$ increased with the increase in the reduction temperature. At 500 ºC, all three desorption regions were identified: two sharp peaks for weakly and moderately adsorbed CO_2; and a broad region from 500 to 700 ºC, attributed to strongly adsorbed CO_2. The effect of reduction temperature on $Co_{2.6}AlO_x$ and $Co_{1.8}Cu_{0.9}AlO_x$ activity was further discussed along with the catalytic tests (section 3.2.2).

Table 3. Calculated CO_2 uptake based on the CO_2-TPD results for the samples.

Catalyst	Reduction Temperature (ºC)	CO_2 uptake ($\mu mol \cdot g^{-1}$)
$Cu_{2.6}AlO_x$	250	10.1
$Co_{1.3}Cu_{1.3}AlO_x$	250	57.2
$Co_{1.8}Cu_{0.9}AlO_x$	250	43.4
	400	84.5
	500	42.9
$Co_{2.6}AlO_x$	250	17.8
	400	31.1
	500	55.5

3.2 Tuning Catalytic Performance

We initially tested the catalysts, namely $Cu_{2.6}AlO_x$, $Cu_{1.3}Co_{1.3}AlO_x$, $Cu_{1.8}Co_{0.9}AlO_x$, and $Co_{2.6}AlO_x$, in the CO_2 hydrogenation reaction at 30 bar, 250 ºC, H_2/CO_2 ratio of 3, gas-hourly space velocity (GHSV) of 14200 $mL \cdot g_{cat}^{-1} \cdot h^{-1}$. Henceforth, the products are coded as CH_4 (methane), CO (carbon monoxide), $C_{2\text{-}5}$ alkanes and alkenes (HCs), methanol, ethanol, and $C_{3+}OH$ (propanol, isopropanol, and other C_{3+} oxygenates).

We evaluated their CO_2 conversion, product selectivity (HCs and oxygenates, CO, and CH_4), HCs and oxygenates (methanol, ethanol, and $C_{3+}OH$) distribution, and space-time yield (STY). For the first test, each sample was reduced at the reaction temperature (250 ºC) in pure hydrogen. Later, we evaluated the effect of changing this temperature of reduction and some reaction parameters. All the results expressed below are summarized in **Table S1** and **Table S2**.

3.2.1 Effect of Co-Cu Ratio

The effect of combining Co and Cu was evidenced by the increase in CO_2 conversion and selectivity towards products of interest. For that, the molar ratios between cobalt and copper in the catalysts can be expressed by the Co/(Co+Cu) ratio. The Co/(Co+Cu) ratios for the samples $Cu_{2.6}AlO_x$, $Cu_{1.3}Co_{1.3}AlO_x$, $Co_{1.8}Cu_{0.9}AlO_x$, and $Co_{2.6}AlO_x$ are, respectively, 0, 0.5, 0.66, and 1. The changes in CO_2 conversion and selectivity towards the different products are expressed in **Figure 5**.

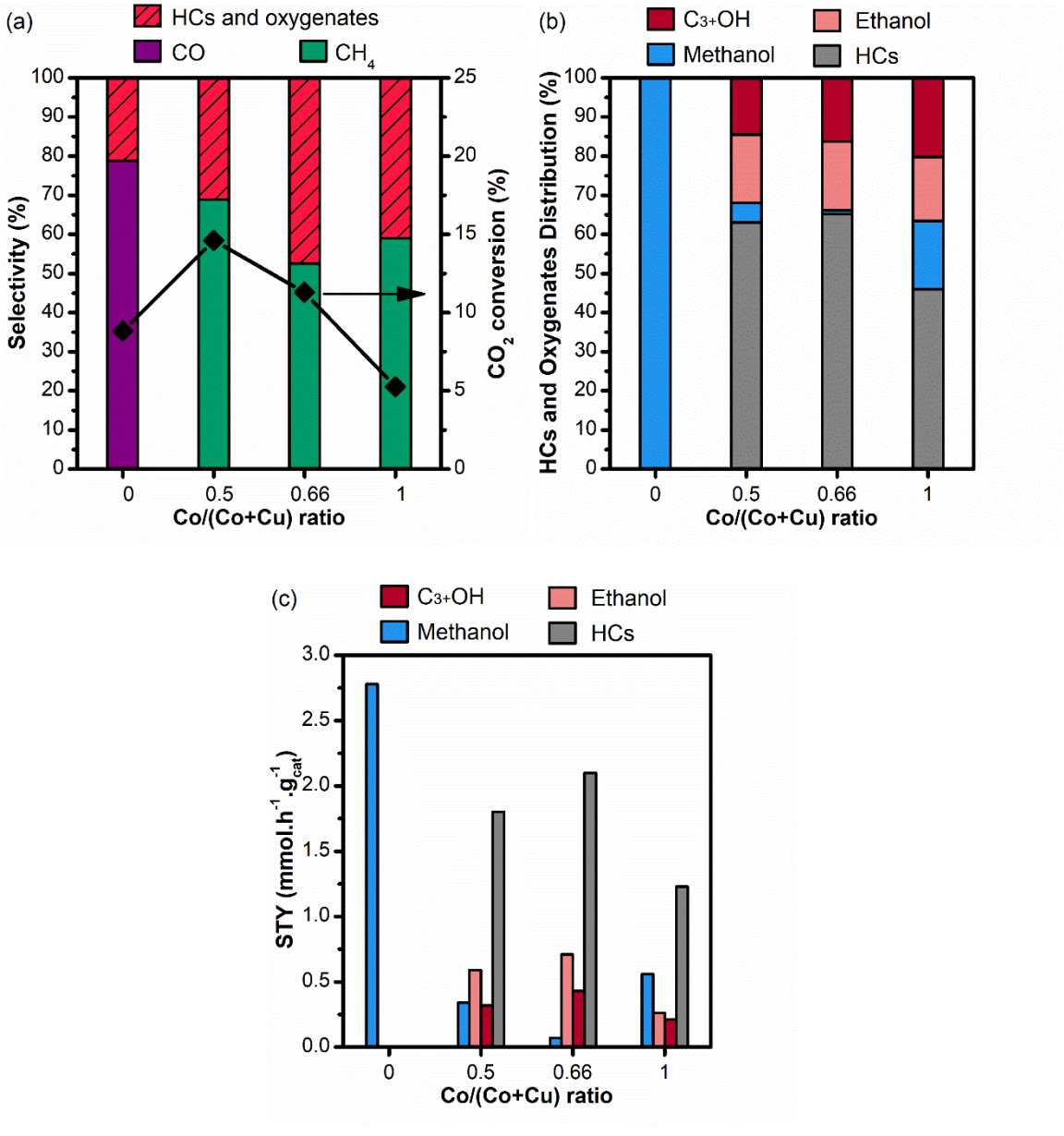

Figure 5. Effect of Co/(Co+Cu) ratio on the selectivity and CO_2 conversion (a), HCs and oxygenates distribution (b), and the STY of products of interest (c) (250 ºC, 30 bar, H_2/CO_2 = 3, GHSV = 14200 $mL \cdot g_{cat}^{-1} \cdot h^{-1}$).

It is possible to observe an increase in CO_2 conversion and selectivity towards products of interest, i.e., hydrocarbons and oxygenates (red), when combining cobalt and copper (**Figure 5a**). Both mixed Co-Cu catalysts, $Cu_{1.3}Co_{1.3}AlO_x$ and $Cu_{1.8}Co_{0.9}AlO_x$, displayed CO_2 conversion above 10%, whereas the values of conversion for the single metal catalysts, $Cu_{2.6}AlO_x$ and $Cu_{2.6}AlO_x$, were below 10%. When comparing the HCs and oxygenates distribution (**Figure 5b**), $Cu_{2.6}AlO_x$ displayed 100% selectivity towards methanol, whereas $Cu_{1.3}Co_{1.3}AlO_x$, $Cu_{1.8}Co_{0.9}AlO_x$, and $Co_{2.6}AlO_x$ produced HCs (gray), ethanol (light red), $C_{3+}OH$ (dark red) and methanol (blue). One can infer that combining Co and Cu increases the yield of higher alcohols and hydrocarbons, implying that the Co-Cu combination favors chain growth. Moreover, $Cu_{1.8}Co_{0.9}AlO_x$, with the Co/(Co+Cu) ratio of 0.66, led to the lowest selectivity towards undesired products, i.e., CH_4 (green) and CO (purple), and the higher yield of both ethanol and $C_{3+}OH$, namely 0.71 and 0.43 $mmol.h^{-1}.g^{-1}$ (**Figure 5c**). This synergic effect between Co and Cu has been previously reported for improving HAs selectivity from syngas [18,31,62,63] and CO_2 hydrogenation [14,19,55]. Subramanian et al. [62], for instance, observed that mixed CoCu particles were more selective towards HAs than CoCu core-shell particles, inferring that both Co and Cu sites must be present on the surface. Sun et al. [18] concluded that each metal played a role in the synthesis of HAs (Cu, activation of surface CO*; and Co, hydrogenation, and chain growth). Moreover, through DFT data and experimental results, Liu et al. [20] observed that there is an ideal Co/(Co+Cu) ratio to maintain optimum CO* surface coverage to produce ethanol. Both Liu et al. [19] and Wang et al. [55] observed the best ethanol selectivity and STY at Co/(Co+Cu) ratios of 0.5 and 0.66.

Considering these results, $Cu_{1.8}Co_{0.9}AlO_x$ displayed the highest STY of HAs and the second-highest CO_2 conversion of all four catalysts; hence we decided to investigate the effect of reduction temperature on this sample. Additionally, we decided to compare the results of $Cu_{2.6}AlO_x$ and $Co_{2.6}AlO_x$ to highlight the Co-Cu catalyst.

3.2.2 Effect of Reduction Temperature

First, we evaluated the influence of the reduction temperature (pure H_2, 30 $ml.min^{-1}$) on the activity of the catalysts. Based on the TPR results and the literature [38,42–44], $Cu_{2.6}AlO_x$ was not

tested with different reduction temperatures, since 250 ºC is sufficient for the reduction and activation of copper. Moreover, the effect of reduction temperatures on $Co_{2.6}AlO_x$ catalytic performance on the CO_2 hydrogenation to higher alcohols is displayed in **Figure 6**. The increase in the reduction temperature led to an increase in CO_2 conversion for $Co_{2.6}AlO_x$, with a decrease in CH_4 selectivity until 400 ºC (**Figure 6a**). Reducing $Co_{2.6}AlO_x$ at 500 ºC led to a noticeable increase in CO_2 conversion with the consequent increase in CH_4 selectivity. The HCs and oxygenates distribution did not change from 400 to 500 ºC (**Figure 6b**). The yield of HAs and HCs was hindered by the reduction at 500 ºC (**Figure 6c**).

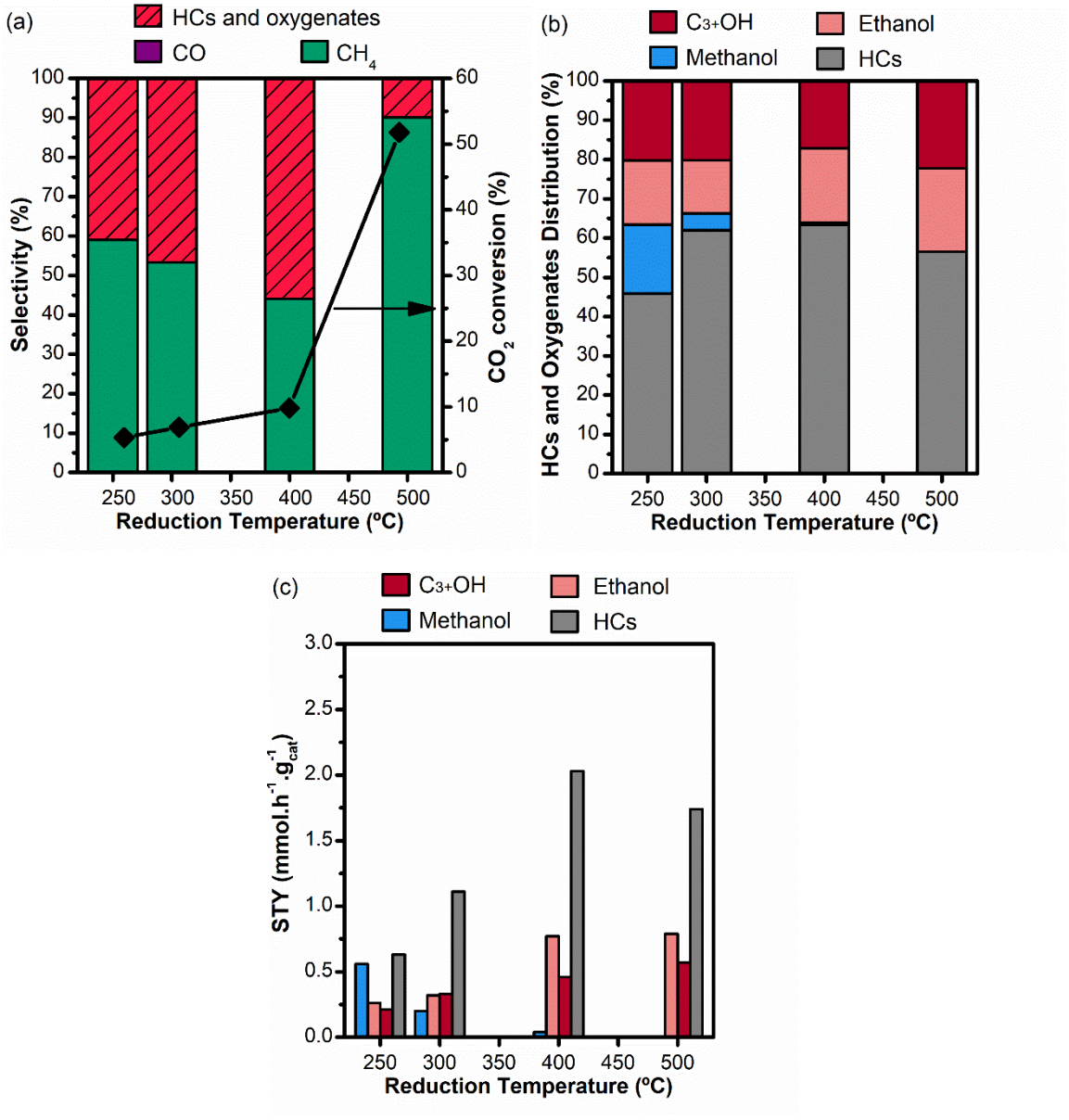

Figure 6. Effect of the reduction temperature on the selectivity and CO_2 conversion (a), HCs and oxygenates distribution (b), and the STY of products of interest (c) of $Co_{2.6}AlO_x$ (250 ºC, 30 bar, H_2/CO_2 = 3, GHSV = 14200 $mL \cdot g_{cat}^{-1} \cdot h^{-1}$).

As previously discussed in the TPR analysis, at temperatures above 400 ºC, the reduction procedure likely leads to the reduction of bulk Co and spinel-like structures [27,31,35]. Excess Co^0 and larger metallic particles can favor methanation reaction [1,2], justifying the increase in CO_2 conversion and CH_4 selectivity. Furthermore, in the CO_2-TPD analyses, the profile of $Co_{2.6}AlO_x$ reduced at 500 ºC displayed remarkable desorption up until 700 ºC, marking strong basicity sites, which promotes methanation [61].

Furthermore, the same reduction temperatures were tested on $Co_{1.8}Cu_{0.9}AlO_x$, and its catalytic performance is presented in **Figure 7**.

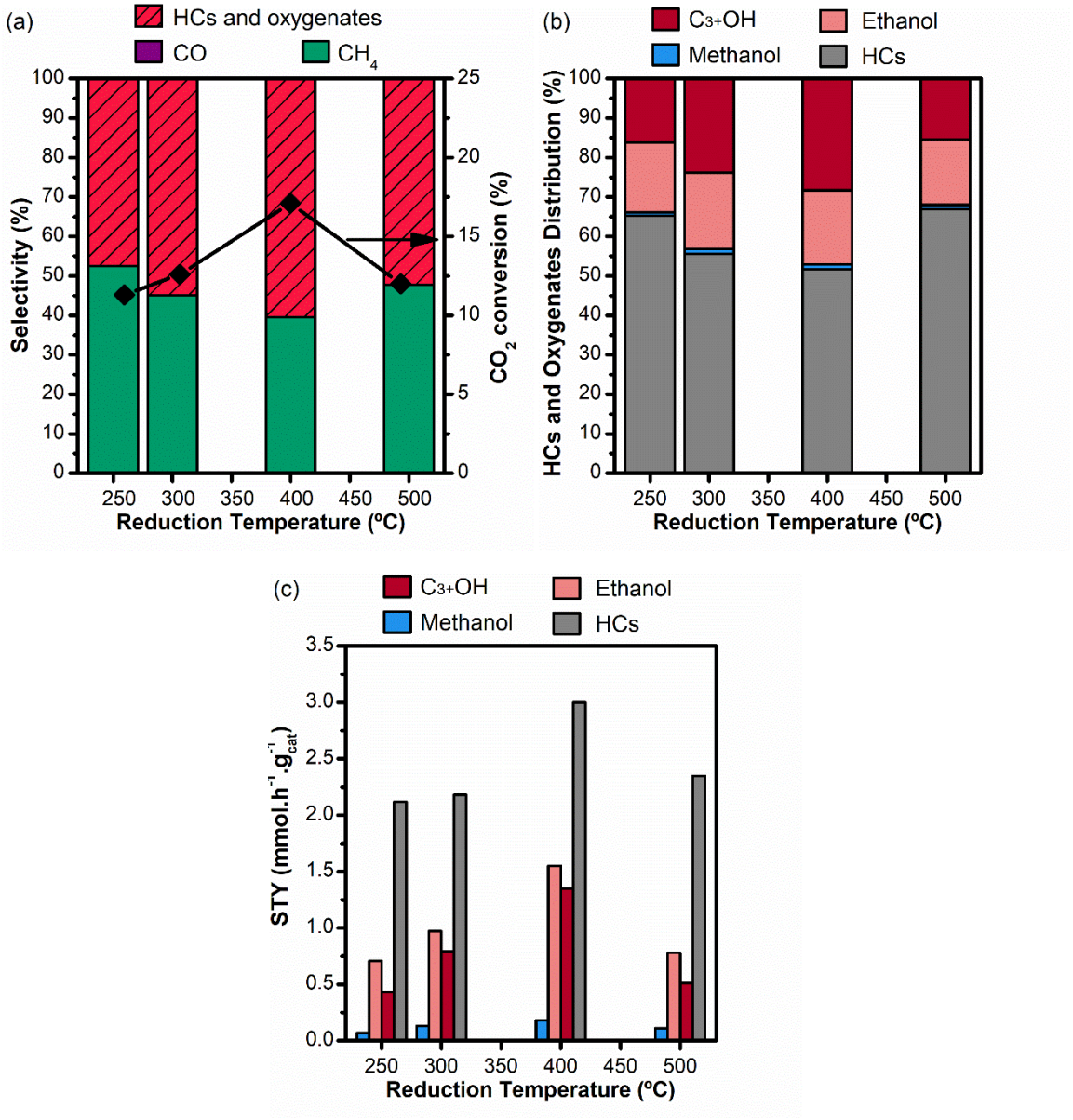

Figure 7. Effect of the reduction temperature on the selectivity and CO_2 conversion (a), HCs and oxygenates distribution (b), and the STY of products of interest (c) of $Co_{1.8}Cu_{0.9}AlO_x$ (250 ºC, 30 bar, H_2/CO_2 = 3, GHSV = 14200 $mL \cdot g_{cat}^{-1} \cdot h^{-1}$).

Similar to $Co_{2.6}AlO_x$, increasing the reduction temperature led to a decrease in CH_4 selectivity for $Co_{1.8}Cu_{0.9}AlO_x$ and an increase in CO_2 conversion up to 400 ºC. Contrastingly, reducing $Co_{1.8}Cu_{0.9}AlO_x$ at 500 ºC led to a decrease in CO_2 conversion (**Figure 7a**) without a significant change in the distribution of HCs and oxygenates (**Figure 7b**). The highest STY of HAs was for the sample reduced at 400 ºC, namely 1.55 and 1.35 $mmol.h^{-1}.g^{-1}$, in that order, for ethanol and $C_{3+}OH$, which represents an increase of approximately 2 and 3 times, respectively, in yield of both HAs

(**Figure 7c**). It is likely that above 400 ºC, the reduction increases the $Co^0/Co^{\delta+}$ ratio on the surface; as a result, hindering the catalyst activity [24,64,65]. As reported, an optimum $Co^0/Co^{\delta+}$ ratio is necessary to tune a cobalt-based catalyst activity and selectivity in the CO_2 hydrogenation reaction [8,24,55,66]. Furthermore, these catalytic test results reflect the CO_2-TPD profile for the different reduction temperatures of $Co_{1.8}Cu_{0.9}AlO_x$ (**Figure 4**). Reducing at 500 ºC reduced by half the calculated CO_2 uptake and led to the disappearance of the peak attributed to moderate basicity and associated with ethanol selectivity [25] and CO_2 hydrogenation activity [15].

A comparison between $Cu_{2.6}AlO_x$, $Co_{1.8}Cu_{0.9}AlO_x$, and $Co_{2.6}AlO_x$ catalytic tests results is shown in **Figure 8**, each catalyst after its best-tested pretreatment, i.e., $Co_{2.6}AlO_x$ and $Co_{1.8}Cu_{0.9}AlO_x$ reduced at 400 ºC, and $Cu_{2.6}AlO_x$ reduced at 250 ºC. Comparatively, the CO_2 conversions for $Cu_{2.6}AlO_x$, $Co_{1.8}Cu_{0.9}AlO_x$, and $Co_{2.6}AlO_x$ at the optimal reduction temperature were 8.8%, 17.2%, and 9.8%, in that order (**Figure 8a**). $Co_{1.8}Cu_{0.9}AlO_x$ reduced at 400 ºC converted nearly twice as much CO_2 as the other two compared catalysts. Moreover, mixing Co-Cu increased the HAs selectivity (28.5%) and hydrocarbons (31.3%). Regarding the yield of products of interest (**Figure 8b**), $Cu_{2.6}AlO_x$ reduced at 250 ºC produced only methanol, circa 2.78 $mmol.h^{-1}.g_{cat}^{-1}$, while the Co-containing catalysts also yielded HAs (C_{2-3}), HCs (C_{2-5}). The yield of HAs and HCs, for $Co_{1.8}Cu_{0.9}AlO_x$ reduced at 400 ºC, were approximately 2.90 and 3.00 $mmol.h^{-1}.g_{cat}^{-1}$, respectively. In that sense, $Co_{1.8}Cu_{0.9}AlO_x$ yielded as much HAs as $Cu_{2.6}AlO_x$ yielded methanol. Henceforth, we evaluated the effect of reaction conditions of $Co_{1.8}Cu_{0.9}AlO_x$ reduced at 400 ºC.

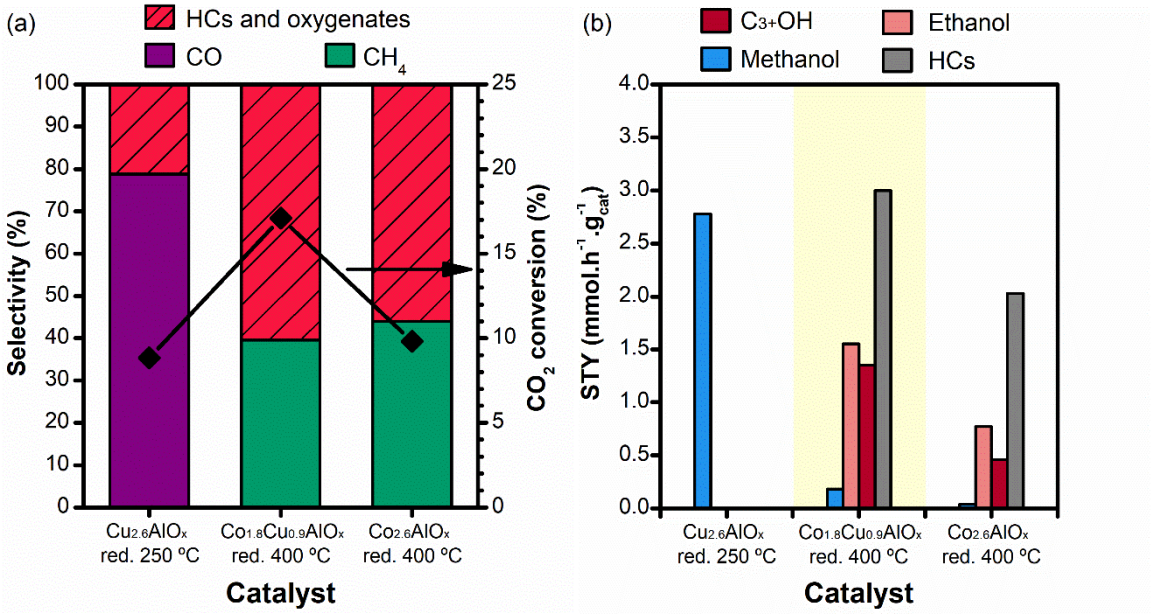

Figure 8. Comparison of the selectivity and CO_2 conversion (a), and the STY of products of interest (b) of the catalysts after the best reduction pretreatment: $Cu_{2.6}AlO_x$ (250 ºC), $Co_{1.8}Cu_{0.9}AlO_x$ (400 ºC), and $Co_{2.6}AlO_x$ (400 ºC), on the CO_2 hydrogenation reaction (250 ºC, 30 bar, $H_2/CO_2 = 3$, GHSV = 14200 $mL \cdot g_{cat}^{-1} \cdot h^{-1}$).

3.2.3 Effect of the Reaction Temperature

We evaluated the influence of the reaction temperature, 50 ºC above and below the previously used temperature (250 ºC), on the activity of $Co_{1.8}Cu_{0.9}AlO_x$ catalytic performance on the CO_2 hydrogenation to HAs, which is displayed in **Figure 9**.

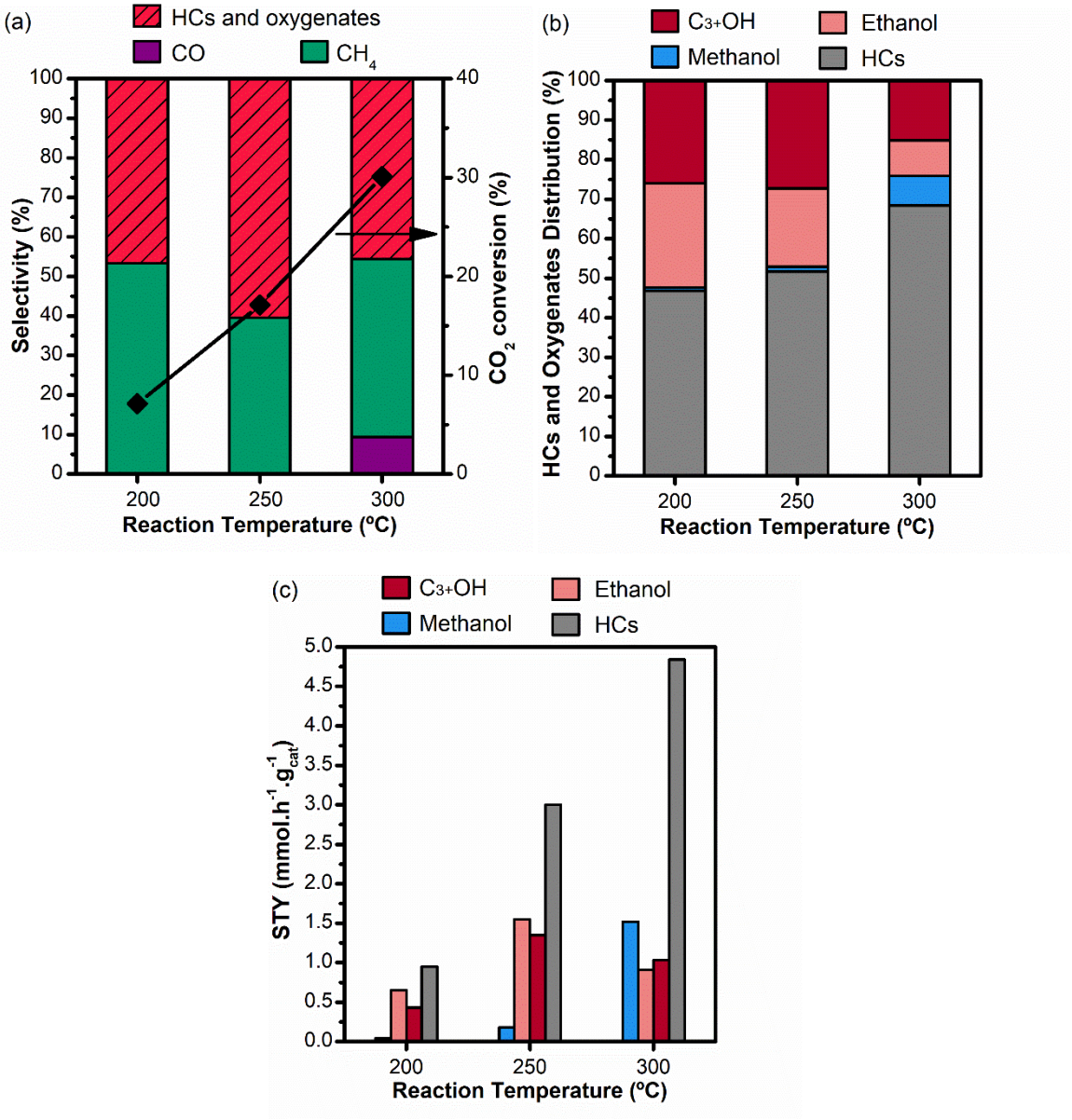

Figure 9. Effect of the reaction temperature on the selectivity and CO_2 conversion (a), HCs and oxygenates distribution (b), and the yield of products of interest (c) of $Co_{1.8}Cu_{0.9}AlO_x$ reduced at 400 ºC (30 bar, H_2/CO_2 = 3, GHSV = 14200 $mL \cdot g_{cat}^{-1} \cdot h^{-1}$).

Increasing the reaction temperature from 200 to 300 ºC increased CO_2 conversion, from 7.1% at 200 ºC to 30.1% at 300 ºC (**Figure 9a**). However, the highest STY for the products of interest (HCs and oxygenates) was at 250 ºC. The increase in reaction temperature to 300 ºC led to CO formation. Moreover, the increase in reaction temperature from 250 to 300 ºC promoted the production of hydrocarbons (**Figure 9b**). Decreasing it from 250 to 200 ºC caused an increase in ethanol selectivity and a decrease in HCs selectivity. In short, even though the increase in reaction

temperature promoted the CO_2 conversion, the yield of higher alcohols was hindered at 300 ºC (**Figure 9b**). Overall, the yield of ethanol and $C_{3+}OH$ was higher at 250 ºC.

The increase in reaction temperature leads to an increase in CO_2 conversion, which can be accompanied by an increase in the yield of higher alcohols [64,67]even when HAs selectivity is hindered by the increase in temperature [24], here evidenced when reaction temperature increased from 200 to 250 ºC. However, the increase in the reaction temperature can also favor the production of side products, such as CO [20], hydrocarbons [68], and methanol [65,69]. As reviewed by Zeng et al. [6], most of the recently reported Co-based catalysts operate well from 140 to 250 ºC, whereas the temperature for Mo-based, Rh-based, and Cu-based catalysts ranges from 200-340 ºC, 240-270 ºC, and 300-350 ºC, respectively.

3.2.4 Effect of the Space Velocity

We tested the effect of space velocity on $Co_{1.8}Cu_{0.9}AlO_x$ catalytic performance, by decreasing the gas-hourly space velocity (GHSV) of the reaction system from 14200 to 10625 $mL.h^{-1}.g_{cat}^{-1}$, and the results are shown in **Figure 10**.

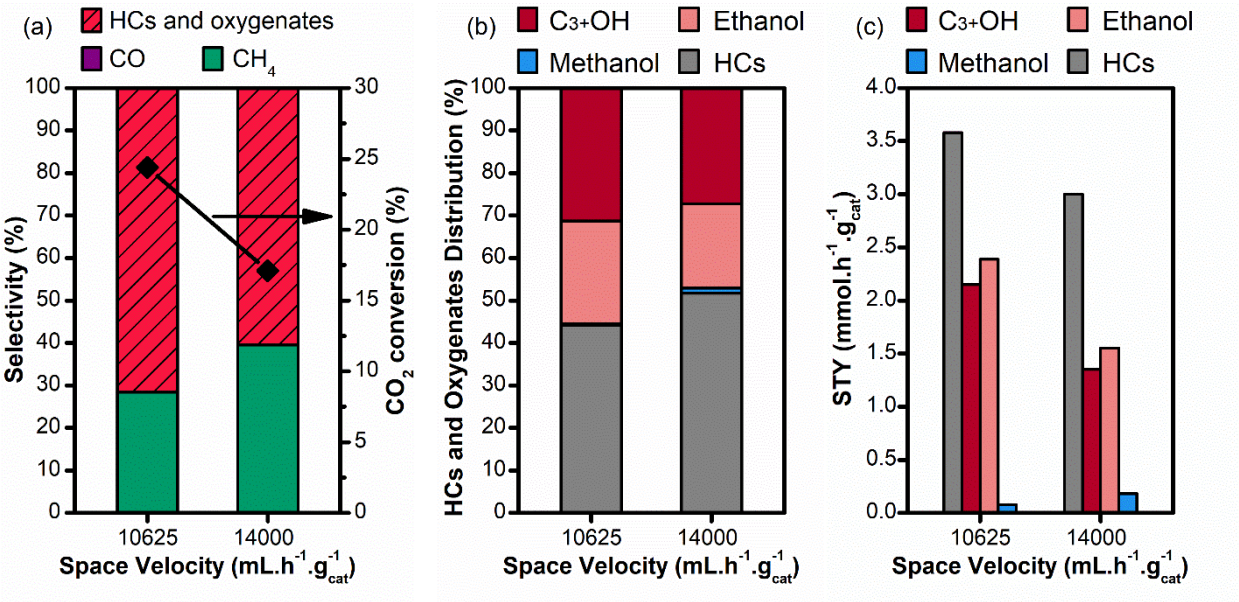

Figure 10. Effect of the space velocity on the selectivity and CO_2 conversion (a), HCs and oxygenates distribution (b), and the yield of products of interest (c) of $Co_{1.8}Cu_{0.9}AlO_x$ reduced at 400 ºC (250 ºC, 30 bar, H_2/CO_2 = 3).

As explained by Si et al. [9], higher space velocity hinders CO insertion, which has slow reaction rate than the C-C coupling and hydrogenation reactions; hence lowering the space velocity could benefit the HAs selectivity. On the other hand, lowering too much the space velocity could lead to a decrease in STY. Overall, this decrease in space velocity was beneficial to the yield of HAs and led to an increase in CO_2 conversion from 17.1% to 24.4%, an increase of roughly 40% (**Figure 10a**). This change also inhibited the production of methane. Moreover, aside from reduced methanol selectivity, the HCs and oxygenates distribution remained roughly the same (**Figure 10b**). This decrease in space velocity promoted the formation of HAs, namely, the yield of ethanol and $C_{3+}OH$ increased approximately 1.5 times each (**Figure 10c**). Xu et al. [10] also observed an increase in CO_2 conversion and a decrease in CO selectivity with the decrease in space velocity, implying that increasing the contact time promotes CO conversion to HAs and HCs. Noteworthy, $Co_{1.8}Cu_{0.9}AlO_x$ did not yield any CO at the space velocity tests.

3.2.5 Effect of the H_2/CO_2 ratio

Next, we also evaluated the effect of changing the H_2/CO_2 ratio from 3 (3:1), as commonly used in most of the recently reported literature [6,9–16], to 1.5 (3:2) on the activity of $Co_{1.8}Cu_{0.9}AlO_x$ catalytic performance on the CO_2 hydrogenation to HAs, which can be seen on **Figure 11**.

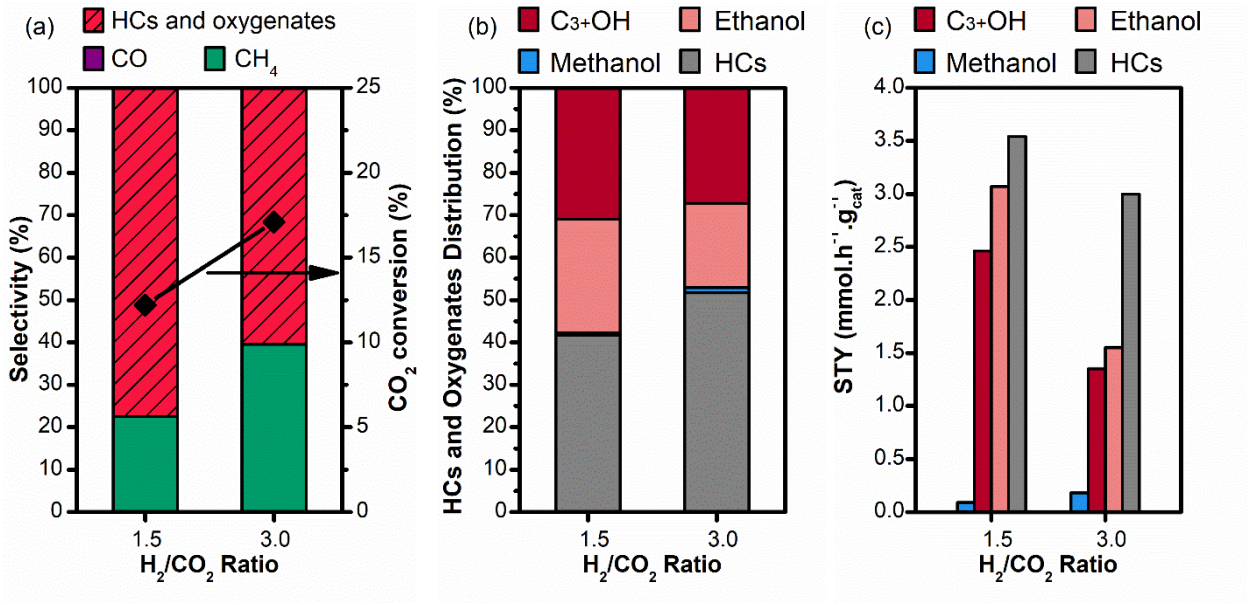

Figure 11. Effect of the H_2/CO_2 ratio on the selectivity and CO_2 conversion (a), HCs and oxygenates distribution (b), and the yield of products of interest (c) of $Co_{1.8}Cu_{0.9}AlO_x$ reduced at 400 ºC (250 ºC, 30 bar, GHSV: 14200 $mL \cdot g_{cat}^{-1} \cdot h^{-1}$).

Reducing the H_2/CO_2 ratio from 3 (3:1) to 1.5 (3:2), we observed a reduction in the nominal value of CO_2 conversion from 17.1% to 12.2%, respectively (**Figure 11a**). However, decreasing the H_2/CO_2 ratio implies reducing the amount of H_2 and increasing the amount of CO_2; therefore, at an H_2/CO_2 ratio of 3:2, more CO_2 was fed to the reactor, namely 60%, more than at H_2/CO_2 ratio of 3:1. Hence, reducing the H_2/CO_2 ratio from 3 (3:1) to 1.5 (3:2) led to an increase in the amount of CO_2 converted, in terms of moles of CO_2 converted per hour at the same space velocity, here evaluated for both tests with different H_2/CO_2 ratio. Methane production is also inhibited, decreasing CH_4 selectivity from 39.5% to 22.5%. This reduction in the H_2/CO_2 ratio also promoted the selectivity towards HAs, namely ethanol, and $C_{3+}OH$ composed approximately 58% of the HCs and oxygenates distribution at H_2/CO_2 ratio of 3:2, compared to 47.1% at H_2/CO_2 ratio of 3:1 (**Figure 11b**). Furthermore, this represents an increase of about 2 and 1.8 times, respectively, to the STY of ethanol and $C_{3+}OH$, whereas the yield of HCs increased by roughly 1.2 times. It is reported that the increase in H_2/CO_2 ratio leads to a decrease in HAs selectivity [25].

3.2.6 Stability of $Co_{1.8}Cu_{0.9}AlO_x$ under different conditions

The 24 h stability profiles of $Co_{1.8}Cu_{0.9}AlO_x$ reduced at 400 ºC are displayed in **Figure 12,** at the initial conditions (250 ºC, 30 bar, H_2/CO_2 = 3, GHSV = 14200 $mL \cdot h^{-1} \cdot g_{cat}^{-1}$), after reducing in space velocity (GHSV = 10625 $mL \cdot h^{-1} \cdot g_{cat}^{-1}$) (**Figure 12b**), and after changing H_2/CO_2 ratio to 1.5 (**Figure 12c**). In all conditions, the carbon balance (C-balance) reaches 95-102% after the first 3 h of reaction, probably due to reactor wash-out after opening. $Co_{1.8}Cu_{0.9}AlO_x$, at the initial conditions (**Figure 12a**), achieves stability after 12 h of reaction. Meanwhile, at GHSV of 10625 $mL \cdot h^{-1} \cdot g_{cat}^{-1}$ (**Figure 12b**), this period was stretched in 3 h. On the other hand, reducing the H_2/CO_2 ratio from 3 to 1.5 (**Figure 12c**) leads to the reactional system reaching stability right after the reactor wash-out. Moreover, after reaching stability, the CO_2 conversion and HAs selectivitydid not change during the 24 h test at that condition, i.e., $Co_{1.8}Cu_{0.9}AlO_x$ did not deactivate. Considering the stability test and yield of products of interest, the H_2/CO_2 ratio change rendered the best catalytic performance for $Co_{1.8}Cu_{0.9}AlO_x$.

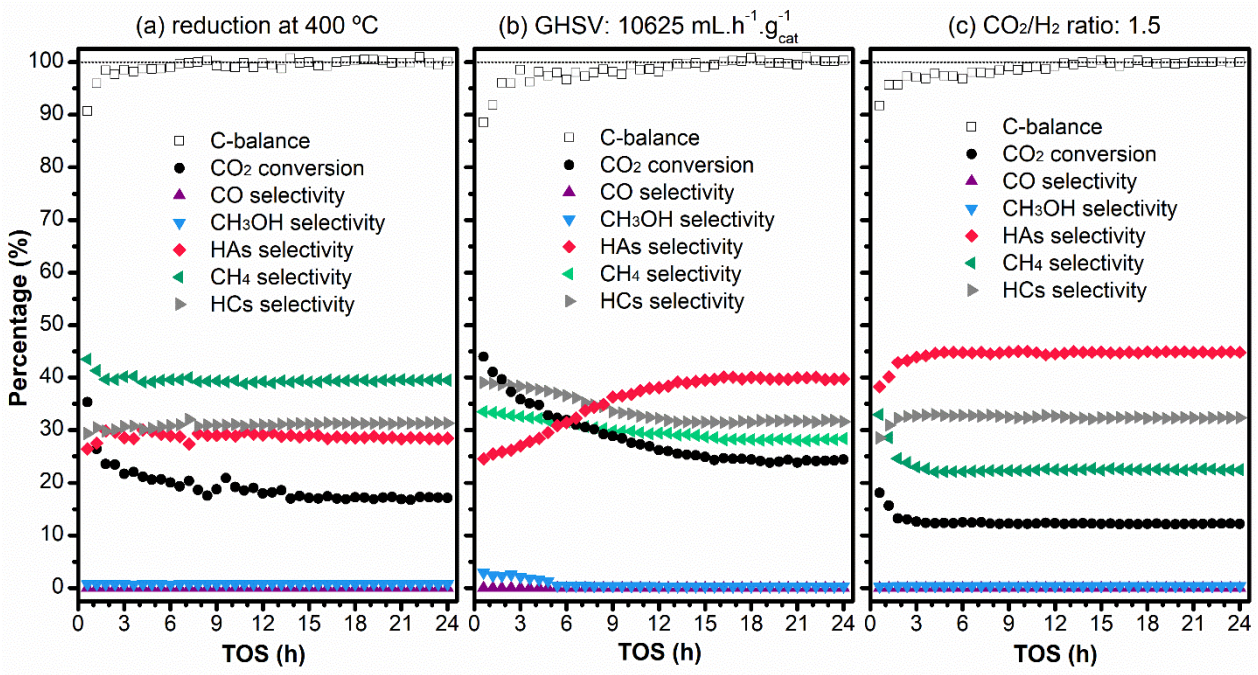

Figure 12. 24 h-TOS of $Co_{1.8}Cu_{0.9}AlO_x$ reduced at 400 ºC at 250 ºC and 30 bar after (a) initial conditions (H_2/CO_2 = 3, GHSV = 14200 $mL \cdot h^{-1} \cdot g_{cat}^{-1}$); (b) decreasing GSHV to 10625 $mL \cdot h^{-1} \cdot g_{cat}^{-1}$ (H_2/CO_2 = 3); and (c) changing H_2/CO_2 ratio to 1.5 (GHSV = 14200 $mL \cdot g_{cat}^{-1} \cdot h^{-1}$).

3.2.7 Final Remarks and Comparisons

Finally, the changes in CO_2 conversion, product selectivity, and STY of each of the tuning steps towards improving $Co_{1.8}Cu_{0.9}AlO_x$ catalytic performance are presented in **Figure 13**. We also compared our best results with the current CO_2 hydrogenation literature, summarized in **Table 4**. In short, there is a progressive decrease in the selectivity of undesired products with each step (**Figure 13a**). $Co_{1.8}Cu_{0.9}AlO_x$ reduced at 250 ºC (reaction condition A) displays HCs and oxygenates selectivity of 47.5%, later increased to 60.5% by tunning the reduction temperature to 400 ºC (reaction condition B). The decrease in space velocity from 14200 to 10625 $mL \cdot h^{-1} \cdot g_{cat}^{-1}$ (reaction condition C) leads to HCs and oxygenates selectivity of 71.6%, whereas changing the H_2/CO_2 ratio from 3 to 1.5 (reaction condition D) increases it to 77.5%. It is worth mentioning that very few of the reviewed works have worked with a space velocity above 6000 $mL \cdot h^{-1} \cdot g_{cat}^{-1}$ [9,13], which is usually done to minimize the selectivity of undesired products, such as CH_4 and CO, yet we still managed to achieve HCs and oxygenates selectivity above 70% working above 10000 $mL \cdot h^{-1} \cdot g_{cat}^{-1}$. The selectivity of $Co_{1.8}Cu_{0.9}AlO_x$ towards undesired products was one of the lowest in the current literature (**Table 4**).

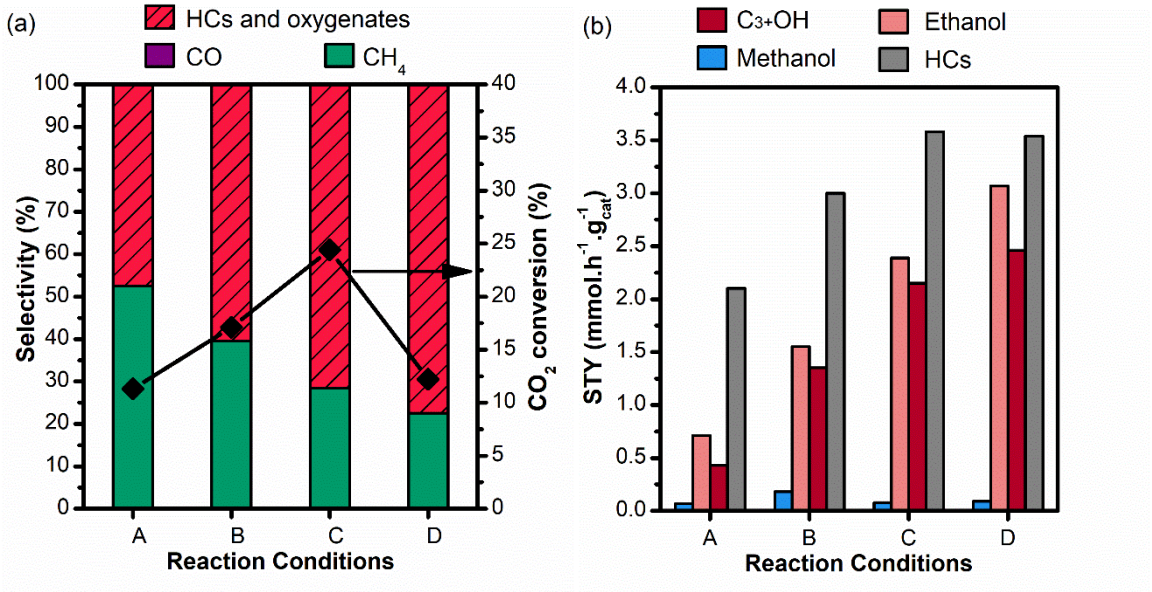

Figure 13. Comparison of $Co_{1.8}Cu_{0.9}AlO_x$ production selectivity and CO_2 conversion (a) and STY (b), at 250 ºC and 30 bar, after each change in reaction conditions: (A) reductive pretreatment at 250 ºC (H_2/CO_2 = 3, GHSV = 14200 $mL \cdot h^{-1} \cdot g_{cat}^{-1}$); (B) reductive pretreatment at 400 ºC(H_2/CO_2 = 3, GHSV = 14200 $mL.h^{-1}.g_{cat}^{-1}$); (C) decreasing GSHV to 10625 $mL.h^{-1}.g_{cat}^{-1}$ (H_2/CO_2 = 3); and (D)

changing H_2/CO_2 ratio to 1.5 (GHSV: 14200 $mL \cdot h^{-1} \cdot g_{cat}^{-1}$).

Table 4. Comparison of the catalytic performance in the current CO_2 hydrogenation literature.

Catalyst	T (ºC)	P (bar)	GHSV (*)	X_{CO_2} (%)	STY (**)	Selectivity (%)					Ref.
						CO	CH_4	HCs (C_{2+})	ROH		
									C_1	C_2	
sp-CuNaFe	310	30	28800	32.3	3.32 [f]	--	--	55.0	--	10	[9]
CZA/K-CMZF	320	50	6000	42.3	2.24 [d]	13.8	--	67.6	1.3	17.4 [d]	[10]
4.6K-CMZF	320	50	6000	30.4	1.47 [d]	30.6	--	52.4	1.3	15.9 [d]	[11]
2.5K5Co-In_2O_3	380	40	2250 [b]	36.6	0.73 [d]	80.8	--	6.5 [c]	1.6 [c]	11.1 [c, d]	[12]
2K20Fe5Rh-SiO_2	250	75	7000	18.4	0.79 [a]	--	46	--	13.8	15.9	[13]
Cu-CoGa-0.4	220	30	6000	17.8	1.35	2.3	43.5	1.9	27.5	23.8	[14]
$CoGa_{1.0}Al_{1.0}O_4/SiO_2$	270	30	3000	4.4	0.3	27.3	--	39.3	13.3	20.1	[15]
25Na-Co/SiO_2	310	50	6000	53.2	1.1	3	61.8	24.3	12.9 [e]		[16]
$Co_{1.8}Cu_{0.9}AlO_x$	250	30	10625	24.4	2.39	0	28.4	31.6	0.3	17.3	This Work
$Co_{1.8}Cu_{0.9}AlO_x$ [g]	250	30	14200	12.2	3.08	0	22.5	32.3	0.4	20.8	This Work

* GHSV expressed in $mL \cdot g_{cat}^{-1} \cdot h^{-1}$ and H_2/CO_2: 3.
** STY of ethanol expressed in $mmol \cdot g_{cat}^{-1} \cdot h^{-1}$.
[a] calculated based on 18.8 $mL \cdot g^{-1} \cdot h^{-1}$ of ethanol, STY after 6h
[b] calculated based on provided flow (37.5 $mL \cdot min^{-1}$) and catalyst mass (1 g)
[c] calculated based on HCs and oxygenates selectivity and distribution
[d] HAs ($C_{2+}OH$) selectivity or STY
[e] Alcohol (ROH) selectivity
[f] calculated based on 153 $mg \cdot g_{cat}^{-1} \cdot h^{-1}$
[g] H_2/CO_2: 3:2 (1.5).

Regarding the space-time yield of $Co_{1.8}Cu_{0.9}AlO_x$, after reduction at 400 ºC, reaction condition B (250 ºC, 30 bar, H_2/CO_2: 3, GHSV: 14200 $mL \cdot h^{-1} \cdot g_{cat}^{-1}$), the yield of ethanol was 1.55 $mmol \cdot h^{-1} \cdot g_{cat}^{-1}$ (STY_{HCs}: 3.00; $STY_{C_{3+}OH}$: 1.35). at these reaction conditions, the ethanol STY of $Co_{1.8}Cu_{0.9}AlO_x$ is higher or comparable to most of the current literature (**Table 4**). After tuning the space velocity, reaction condition C (250 ºC, 30 bar, H_2/CO_2: 3, GHSV: 10625 $mL \cdot h^{-1} \cdot g_{cat}^{-1}$), the ethanol STY reached 2.39 $mmol.h^{-1}.g_{cat}^{-1}$ (STY_{HCs}: 3.24; $STY_{C_{3+}OH}$: 2.15). Meanwhile, tuning the H_2/CO_2 ratio, reaction condition D (250 ºC, 30 bar, H_2/CO_2: 1.5, GHSV: 14000 $mL \cdot h^{-1} \cdot g_{cat}^{-1}$), led to an ethanol STY of 3.08 $mmol \cdot h^{-1} \cdot g_{cat}^{-1}$ (STY_{HCs}: 3.54; $STY_{C_{3+}OH}$: 2.46).

Comparatively, Xu et al. [10] reported a tandem catalyst composed of a CuZnAl catalyst to favor CO formation, and a K-CuMgZnFe catalyst to favor HAs formation reaching STY of 2.24

mmol.h^{-1}.g_{cat}^{-1} (310 ºC, 50 bar, H_2/CO_2: 3, GHSV: 6000 mL·h^{-1}·g_{cat}^{-1}) for higher alcohols (ethanol and C_{3+} oxygenates). Even though the tandem catalyst displayed elevated CO_2 conversion (42.3%), the higher alcohol selectivity (17.4%) was lower than the one displayed by of $Co_{1.8}Cu_{0.9}AlO_x$ (39.7% for reaction condition C and 44.8% for reaction condition D). In the end, $Co_{1.8}Cu_{0.9}AlO_x$ ethanol STY in both reaction conditions was similar or higher than the higher alcohol (ethanol and C_{3+} oxygenates) STY displayed by the tandem catalysts working at a much higher pressure (50 bar). Furthermore, Si et al. [9] reported a sputtering CuNaFe catalyst with high STY of alkene of 680 mg·h^{-1}·g_{cat}^{-1} and ethanol of 153 mg·h^{-1}·g_{cat}^{-1} (310 ºC, 30 bar, H_2/CO_2: 3, GHSV: 28800 mL·h^{-1}·g_{cat}^{-1}), which converts to 3.32 mmol·h^{-1}·g_{cat}^{-1} ($MM_{ethanol}$: 46.07 g·mol^{-1}). The ethanol STY of sp-CuNaFe was similar to the displayed by $Co_{1.8}Cu_{0.9}AlO_x$ at reaction condition D (H_2/CO_2: 1.5). The sp-CuNaFe catalyst operates at double the GHSV of our experiments. It is also important to mention that, at reaction condition D, we reduced the amount of H_2 used in the process, ergo diminishing its cost. Noteworthy, $Co_{1.8}Cu_{0.9}AlO_x$, under certain conditions, displays one of the highest ethanol STY of the literature, to the best of our knowledge.

Lastly, it is essential to acknowledge that the CO_2 hydrogenation reaction to ethanol and other higher alcohols (HAs) is currently rated at Technology Readiness Level (TRL) 1-2, indicating that it is transitioning from pure to applied research [70]. Therefore, one should expect few reports on catalysts, especially non-noble-based ones, with high selectivity to ethanol or other HAs, due to the existing challenges in the CO_2 hydrogenation process. Achieving high yields of products is challenging due to the thermodynamic stability of CO_2, which often requires high temperatures, pressures, excess overpotentials, or the use of catalysts with low availability and high costs [3,71]. However, progress is being made over time as new active materials demonstrate the potential to increase yield and selectivity to alcohols, making this process more feasible.

In this context, our work presents a non-noble-based catalyst that, under mild conditions, displayed conversion rates comparable to current results while showing superior selectivity and yield towards higher alcohols, particularly ethanol. This achievement represents a significant advancement in the field and offers promising potential for the synthesis of higher alcohols from CO_2.

As we advance toward higher TRLs, it becomes crucial to consider implementation aspects,

including addressing separation and recycling steps, and their impact on the process's cost and emission reduction efficiency. These factors play a significant role in ensuring the practical viability and sustainability of the CO_2 hydrogenation to higher alcohols, making it essential to explore efficient and cost-effective approaches for separation, recycling, and overall process optimization.

4. Conclusion

Overall, Co-Cu-Al proves to be a performant catalyst to produce ethanol (and potential other oxygenates) via the CO_2 hydrogenation reaction at mild reaction conditions. $Co_{1.8}Cu_{0.9}AlO_x$, at the best-tested reaction conditions (250 ºC, 30 bar, H_2/CO_2: 1.5, GHSV = 14000 $mL \cdot h^{-1} \cdot g_{cat}^{-1}$), displays very low CH_4 selectivity (22.5%) and very high selectivity towards products of interest (77.5), i.e., HCs and oxygenate. The space-time yields in these conditions are 3.54, 3.08, and 2.46 $mmol \cdot h^{-1} \cdot g_{cat}^{-1}$ for hydrocarbons (C_{2-5}), ethanol, and $C_{3+}OH$, respectively. The ethanol STY is one the highest among related studies, that is, for continuous reactors. The yield of hydrocarbons and $C_{3+}OH$ also represents potential pathways for other utilizations of such catalysts. Finally, tuning the catalyst proves to be a viable alternative to improve the catalytic activity, as the CO_2 hydrogenation reaction is shown to be sensitive to space velocity and H_2/CO_2 ratio, among other reaction conditions. The overall gain in ethanol space-time yield from the reaction condition A ($Co_{1.8}Cu_{0.9}AlO_x$ reduced at 250ºC – 250 ºC, 30 bar, H_2/CO_2: 3, GHSV: 14000 $mL \cdot h^{-1} \cdot g_{cat}^{-1}$) to reaction condition D ($Co_{1.8}Cu_{0.9}AlO_x$ reduced at 400ºC – 250 ºC, 30 bar, H_2/CO_2 = 1.5, GHSV = 14000 $mL \cdot h^{-1} \cdot g_{cat}^{-1}$) was of 4.3-fold. In short, this work shed light on designing and tuning high-efficiency Co-Cu bimetallic catalysts for converting CO_2 into chemicals of industrial interest.

5. Acknowledgments

The authors would like to acknowledge CAPES (Coordenação de Aperfeiçoamento de Pessoal de Nível Superior – Brasil) – Finance Code 001 and COFECUB (Comitê Francês de Avaliação da Cooperação Universitária com o Brasil – Ph-C 912/18), European Union (ERDF) and Région Nouvelle Aquitaine for the financial support, as well as UFRJ (Universidade Federal do Rio de Janeiro), the Université de Poitiers and CNRS (Centre National de la Recherche Scientifique) for letting this research to be developed in their facilities and with the aid. The authors also would like to thank LabTecH2 (Laboratório de Tecnologia do Hidrogênio) at UFRJ for the XRD analyses.

6. References

[1] W. Wang, S. Wang, X. Ma, J. Gong, Recent advances in catalytic hydrogenation of carbon dioxide, Chem Soc Rev. 40 (2011) 3703–3727. https://doi.org/10.1039/c1cs15008a.

[2] W. Li, H. Wang, X. Jiang, J. Zhu, Z. Liu, X. Guo, C. Song, A short review of recent advances in CO 2 hydrogenation to hydrocarbons over heterogeneous catalysts, RSC Adv. 8 (2018) 7651–7669. https://doi.org/10.1039/c7ra13546g.

[3] A.D.N. Kamkeng, M. Wang, J. Hu, W. Du, F. Qian, Transformation technologies for CO2 utilisation: Current status, challenges and future prospects, Chemical Engineering Journal. 409 (2021). https://doi.org/10.1016/j.cej.2020.128138.

[4] W.N.R.W. Isahak, L.M. Shaker, A. Al-Amiery, Oxygenated Hydrocarbons from Catalytic Hydrogenation of Carbon Dioxide, Catalysts. 13 (2023). https://doi.org/10.3390/catal13010115.

[5] S.S. Ali, S.S. Ali, N. Tabassum, A review on CO2 hydrogenation to ethanol: Reaction mechanism and experimental studies, J Environ Chem Eng. 10 (2022). https://doi.org/10.1016/j.jece.2021.106962.

[6] F. Zeng, C. Mebrahtu, X. Xi, L. Liao, J. Ren, J. Xie, H.J. Heeres, R. Palkovits, Catalysts design for higher alcohols synthesis by CO2 hydrogenation: Trends and future perspectives, Appl Catal B. 291 (2021). https://doi.org/10.1016/j.apcatb.2021.120073.

[7] Y. He, S. Liu, W. Fu, C. Wang, C. Mebrahtu, R. Sun, F. Zeng, Thermodynamic Analysis of CO2Hydrogenation to Higher Alcohols (C2-4OH): Effects of Isomers and Methane, ACS Omega. (2022). https://doi.org/10.1021/acsomega.2c00502.

[8] S. Liu, Y. He, W. Fu, J. Chen, J. Ren, L. Liao, R. Sun, Z. Tang, C. Mebrahtu, F. Zeng, Hetero-site cobalt catalysts for higher alcohols synthesis by CO2hydrogenation: A review, Journal of CO2 Utilization. 67 (2023). https://doi.org/10.1016/j.jcou.2022.102322.

[9] Z. Si, L. Wang, Y. Han, J. Yu, Q. Ge, C. Zeng, J. Sun, Synthesis of Alkene and Ethanol in CO2 Hydrogenation on a Highly Active Sputtering CuNaFe Catalyst, ACS Sustain Chem Eng. 10 (2022) 14972–14979. https://doi.org/10.1021/acssuschemeng.2c05450.

[10] D. Xu, H. Yang, X. Hong, G. Liu, S.C. Edman Tsang, Tandem Catalysis of Direct CO2Hydrogenation to Higher Alcohols, ACS Catal. 11 (2021) 8978–8984. https://doi.org/10.1021/acscatal.1c01610.

[11] D. Xu, M. Ding, X. Hong, G. Liu, Mechanistic aspects of the role of K promotion on Cu−Fe-based catalysts for higher alcohol synthesis from CO2 hydrogenation, ACS Catal. 10 (2020) 14516–14526. https://doi.org/10.1021/acscatal.0c03575.

[12] T. Witoon, T. Numpilai, S. Nijpanich, N. Chanlek, P. Kidkhunthod, C.K. Cheng, K.H. Ng, D.V.N. Vo, S. Ittisanronnachai, C. Wattanakit, M. Chareonpanich, J. Limtrakul, Enhanced CO2 hydrogenation to higher alcohols over K-Co promoted In2O3 catalysts, Chemical Engineering Journal. 431 (2022). https://doi.org/10.1016/j.cej.2021.133211.

[13] A. Goryachev, A. Pustovarenko, G. Shterk, N.S. Alhajri, A. Jamal, M. Albuali, L. van Koppen, I.S. Khan, A. Russkikh, A. Ramirez, T. Shoinkhorova, E.J.M. Hensen, J. Gascon, A Multi-Parametric Catalyst Screening for CO2 Hydrogenation to Ethanol, ChemCatChem. 13 (2021) 3324–3332. https://doi.org/10.1002/cctc.202100302.

[14] G. Zhang, G. Fan, L. Zheng, F. Li, Ga-Promoted CuCo-Based Catalysts for Efficient CO2 Hydrogenation to Ethanol: The Key Synergistic Role of Cu-CoGaOx Interfacial Sites, ACS Appl Mater Interfaces. 14 (2022) 35569–35580. https://doi.org/10.1021/acsami.2c07252.

[15] K. An, S. Zhang, H. Wang, N. Li, Z. Zhang, Y. Liu, Co0−Coδ+ active pairs tailored by Ga-Al-O spinel for CO2-to-ethanol synthesis, Chemical Engineering Journal. 433 (2022) 134606. https://doi.org/10.1016/j.cej.2022.134606.

[16] S. Zhang, Z. Wu, X. Liu, Z. Shao, L. Xia, L. Zhong, H. Wang, Y. Sun, Tuning the interaction between Na and Co2C to promote selective CO2 hydrogenation to ethanol, Appl Catal B. 293 (2021). https://doi.org/10.1016/j.apcatb.2021.120207.

[17] M. Wang, G. Zhang, J. Zhu, W. Li, J. Wang, K. Bian, Y. Liu, F. Ding, C. Song, X. Guo, Unraveling the tunable selectivity on cobalt oxide and metallic cobalt sites for CO2 hydrogenation, Chemical Engineering Journal. 446 (2022). https://doi.org/10.1016/j.cej.2022.137217.

[18] K. Sun, X. Gao, Y. Bai, M. Tan, G. Yang, Y. Tan, Synergetic catalysis of bimetallic copper-cobalt nanosheets for direct synthesis of ethanol and higher alcohols from syngas, Catal Sci Technol. 8 (2018) 3936–3947. https://doi.org/10.1039/c8cy01074a.

[19] S. Liu, C. Yang, S. Zha, D. Sharapa, F. Studt, Z.J. Zhao, J. Gong, Moderate Surface Segregation Promotes Selective Ethanol Production in CO2 Hydrogenation Reaction over CoCu Catalysts, Angewandte Chemie - International Edition. 61 (2022). https://doi.org/10.1002/anie.202109027.

[20] S. Liu, H. Zhou, Q. Song, Z. Ma, Synthesis of higher alcohols from CO 2 hydrogenation over Mo–Co–K sulfide-based catalysts, J Taiwan Inst Chem Eng. 76 (2017) 18–26. https://doi.org/10.1016/j.jtice.2017.04.007.

[21] M. Ao, G.H. Pham, J. Sunarso, F. Li, Y. Jin, S. Liu, Effects of alkali promoters on tri-metallic Co-Ni-Cu-based perovskite catalyst for higher alcohol synthesis from syngas, Catal Today. 355 (2020) 26–34. https://doi.org/10.1016/j.cattod.2019.06.061.

[22] R.A. Iloy, K. Jalama, Effect of operating temperature, pressure and potassium loading on the performance of silica-supported Cobalt catalyst in CO2 hydrogenation to hydrocarbon fuel, Catalysts. 9 (2019). https://doi.org/10.3390/catal9100807.

[23] W. Aslam, J.N. Beltramini, L.A. Atanda, N.R. Batalha, T.U. Schülli, M. Konarova, The catalytic activity of KMoCo carbon spheres for higher alcohols synthesis from syngas, Appl Catal A Gen. 605 (2020) 117803. https://doi.org/10.1016/j.apcata.2020.117803.

[24] L. Wang, L. Wang, J. Zhang, X. Liu, H. Wang, W. Zhang, Q. Yang, J. Ma, X. Dong, S.J. Yoo, J. Kim, X. Meng, F. Xiao, Selective Hydrogenation of CO2 to Ethanol over Cobalt Catalysts, Angewandte Chemie - International Edition. 130 (2018) 6212–6216. https://doi.org/10.1002/ange.201800729.

[25] K. An, S. Zhang, J. Wang, Q. Liu, Z. Zhang, Y. Liu, A highly selective catalyst of Co/La4Ga2O9 for CO2 hydrogenation to ethanol, Journal of Energy Chemistry. 56 (2021) 486–495. https://doi.org/10.1016/j.jechem.2020.08.045.

[26] D. Xu, Y. Wang, M. Ding, X. Hong, G. Liu, S.C.E. Tsang, Advances in higher alcohol synthesis from CO2 hydrogenation, Chem. 7 (2021) 849–881. https://doi.org/10.1016/j.chempr.2020.10.019.

[27] D. dos S. Lima, Y.R. Dias, O.W. Perez-Lopez, CO2methanation over Ni-Al and Co-Al LDH-derived catalysts: The role of basicity, Sustain Energy Fuels. 4 (2020) 5747–5756. https://doi.org/10.1039/d0se01059f.

[28] Z. Liu, X. Gao, B. Liu, W. Song, Q. Ma, T. sheng Zhao, X. Wang, J.W. Bae, X. Zhang, J. Zhang, Highly stable and selective layered Co-Al-O catalysts for low-temperature CO2 methanation, Appl Catal B. 310 (2022). https://doi.org/10.1016/j.apcatb.2022.121303.

[29] L. Wang, S. He, L. Wang, Y. Lei, X. Meng, F.-S. Xiao, Cobalt–Nickel Catalysts for Selective Hydrogenation of Carbon Dioxide into Ethanol, ACS Catal. 9 (2019) 11335–11340. https://doi.org/10.1021/acscatal.9b04187.

[30] R. Benhiti, A. Ait Ichou, A. Zaghloul, R. Aziam, G. Carja, M. Zerbet, F. Sinan, M. Chiban, Synthesis, characterization, and comparative study of MgAl-LDHs prepared by standard coprecipitation and urea hydrolysis methods for phosphate removal, Environmental Science and Pollution Research. 27 (2020) 45767–45774. https://doi.org/10.1007/s11356-020-10444-5.

[31] C. Göbel, S. Schmidt, C. Froese, Q. Fu, Y.T. Chen, Q. Pan, M. Muhler, Structural evolution of bimetallic Co-Cu catalysts in CO hydrogenation to higher alcohols at high pressure, J Catal. 383 (2020) 33–41. https://doi.org/10.1016/j.jcat.2020.01.004.

[32] K. Kupková, P. Topka, J. Balabánová, M. Koštejn, K. Jirátová, J.-M. Giraudon, J.-F. Lamonier, J. Maixner, F. Kovanda, Cobalt-Copper Oxide Catalysts for VOC Abatement: Effect of Co:Cu Ratio on Performance in Ethanol Oxidation, Catalysts. 13 (2023) 107. https://doi.org/10.3390/catal13010107.

[33] K. Jirátová, F. Kovanda, J. Ludvíková, J. Balabánová, J. Klempa, Total oxidation of ethanol over layered double hydroxide-related mixed oxide catalysts: Effect of cation composition, Catal Today. 277 (2016) 61–67. https://doi.org/10.1016/j.cattod.2015.10.036.

[34] L. Obalová, K. Karásková, K. Jirátová, F. Kovanda, Effect of potassium in calcined Co-Mn-Al layered double hydroxide on the catalytic decomposition of N2O, Appl Catal B. 90 (2009) 132–140. https://doi.org/10.1016/j.apcatb.2009.03.002.

[35] K. Karásková, K. Pacultová, K. Jirátová, D. Fridrichová, M. Koštejn, L. Obalová, K-Modified Co–Mn–Al Mixed Oxide—Effect of Calcination Temperature on N2O Conversion in the Presence of H2O and NOx, Catalysts. 10 (2020) 1134. https://doi.org/10.3390/catal10101134.

[36] F. Kefif, K. Ezziane, A. Bahmani, N. Bettahar, S. Mayouf, Evans Blue dye removal from contaminated water on calcined and uncalcined Cu-Al-CO3 layered double hydroxide materials prepared by coprecipitation, Bulletin of Materials Science. 42 (2019). https://doi.org/10.1007/s12034-018-1694-z.

[37] T.P. Sulmonetti, B. Hu, S. Lee, P.K. Agrawal, C.W. Jones, Reduced Cu-Co-Al Mixed Metal Oxides for the Ring-Opening of Furfuryl Alcohol to Produce Renewable Diols, ACS Sustain Chem Eng. 5 (2017) 8959–8969. https://doi.org/10.1021/acssuschemeng.7b01769.

[38] C.D.O.P. Teixeira, S.D.S. Montani, L.A. Palacio, F.M.Z. Zotin, The effect of preparation methods on the thermal and chemical reducibility of Cu in Cu-Al oxides, Dalton Transactions. 47 (2018) 10989–11001. https://doi.org/10.1039/c8dt01150h.

[39] C. Wan, X. Wei, G. Cai, D. Li, Y. Zhan, Y. Xiao, L. Jiang, Hydrotalcite-derived aluminum-doped cobalt oxides for catalytic benzene combustion: Effect of calcination atmosphere, Molecular Catalysis. 520 (2022). https://doi.org/10.1016/j.mcat.2022.112160.

[40] C. Chen, L. Liu, Y. Li, W. Li, L. Zhou, Y. Lan, Y. Li, Insight into heterogeneous catalytic degradation of sulfamethazine by peroxymonosulfate activated with CuCo2O4 derived from bimetallic oxalate, Chemical Engineering Journal. 384 (2020) 123257. https://doi.org/10.1016/j.cej.2019.123257.

[41] Y. Wei, S. Li, J. Jing, M. Yang, C. Jiang, W. Chu, Synthesis of Cu–Co Catalysts for Methanol Decomposition to Hydrogen Production via Deposition–Precipitation with Urea Method, Catal Letters. 149 (2019) 2671–2682. https://doi.org/10.1007/s10562-019-02731-9.

[42] W. Kim, K.K. Mohaideen, D.J. Seo, W.L. Yoon, Methanol-steam reforming reaction over Cu-Al-based catalysts derived from layered double hydroxides, Int J Hydrogen Energy. 42 (2017) 2081–2087. https://doi.org/10.1016/j.ijhydene.2016.11.014.

[43] H.R. Prakruthi, B.M. Chandrashekara, J.P. Jai, Y.S. Bhat, Hydrogenation efficiency of highly porous Cu-Al oxides derived from dealuminated LDH in the conversion of furfural to furfuryl alcohol, Journal of Industrial and Engineering Chemistry. 62 (2018) 96–105. https://doi.org/10.1016/j.jiec.2017.12.048.

[44] C.L.O. Corrêa, Y.E. Licea, L.A. Palacio, F.M.Z. Zotin, Effect of composition and thermal treatment in catalysts derived from Cu-Al hydrotalcites-like compounds in the NO reduction by CO, Catal Today. 289 (2017) 133–142. https://doi.org/10.1016/j.cattod.2016.08.023.

[45] Q. Zhao, Y. Ge, K. Fu, N. Ji, C. Song, Q. Liu, Oxidation of acetone over Co-based catalysts derived from hierarchical layer hydrotalcite: Influence of Co/Al molar ratios and calcination temperatures, Chemosphere. 204 (2018) 257–266. https://doi.org/10.1016/j.chemosphere.2018.03.198.

[46] R. Ramos, A. Grigoropoulos, N. Perret, M. Zanella, A.P. Katsoulidis, T.D. Manning, J.B. Claridge, M.J. Rosseinsky, Selective conversion of 5-hydroxymethylfurfural to cyclopentanone derivatives over Cu-Al2O3 and Co-Al2O3 catalysts in water, Green Chemistry. 19 (2017) 1701–1713. https://doi.org/10.1039/c7gc00315c.

[47] F. Teodorescu, A.I. Slabu, O.D. Pavel, R. Zăvoianu, A comparative study on the catalytic activity of ZnAl, NiAl, and CoAl mixed oxides derived from LDH obtained by mechanochemical method in the synthesis of 2-methylpyrazine, Catal Commun. 133 (2020). https://doi.org/10.1016/j.catcom.2019.105829.

[48] N. Aider, F. Touahra, F. Bali, B. Djebarri, D. Lerari, K. Bachari, D. Halliche, Improvement of catalytic stability and carbon resistance in the process of CO2 reforming of methane by CoAl and CoFe hydrotalcite-derived catalysts, Int J Hydrogen Energy. 43 (2018) 8256–8266. https://doi.org/10.1016/j.ijhydene.2018.03.118.

[49] R. Berenguer, C. Quijada, A. la Rosa-Toro, E. Morallón, Electro-oxidation of cyanide on active and non-active anodes: Designing the electrocatalytic response of cobalt spinels, Sep Purif Technol. 208 (2019) 42–50. https://doi.org/10.1016/j.seppur.2018.05.024.

[50] P. Paknahad, M. Askari, M. Ghorbanzadeh, Characterization of nanocrystalline CuCo2O4 spinel prepared by sol–gel technique applicable to the SOFC interconnect coating, Applied Physics A. 119 (2015) 727–734. https://doi.org/10.1007/s00339-015-9021-7.

[51] B. Kreitz, G.D. Wehinger, C.F. Goldsmith, T. Turek, Microkinetic Modeling of the CO2Desorption from Supported Multifaceted Ni Catalysts, Journal of Physical Chemistry C. 125 (2021) 2984–3000. https://doi.org/10.1021/acs.jpcc.0c09985.

[52] J.A. Delgado, J.L. Sotelo, J.M. Gómez, P. Gómez, Estimation of Adsorption Parameters from Temperature-Programmed Desorption Thermograms: Application to the Adsorption of Carbon Dioxide onto Alumina, Adsorption Science & Technology. 25 (2007) 113–128. https://doi.org/10.1260/026361707782398146.

[53] J.A. Delgado, J.M. Gómez, Estimation of adsorption parameters from temperature-programed-desorption thermograms: Application to the adsorption of carbon dioxide onto Na-and H-mordenite, Langmuir. 21 (2005) 9555–9561. https://doi.org/10.1021/la050966u.

[54] M. Xu, E. Iglesia, Readsorption and Adsorption-Assisted Desorption of CO2 on Basic Solids, J Phys Chem B. 102 (1998) 961–966. https://doi.org/10.1021/jp972200b.

[55] Z. Wang, C. Yang, X. Li, X. Song, C. Pei, Z.J. Zhao, J. Gong, The role of CO2 dissociation in CO2 hydrogenation to ethanol on CoCu/silica catalysts, Nano Res. (2022). https://doi.org/10.1007/s12274-022-5092-x.

[56] Z. Shi, H. Yang, P. Gao, X. Li, L. Zhong, H. Wang, H. Liu, W. Wei, Y. Sun, Direct conversion of CO2 to long-chain hydrocarbon fuels over K-promoted CoCu/TiO2 catalysts, Catal Today. 311 (2018) 65–73. https://doi.org/10.1016/j.cattod.2017.09.053.

[57] T.H. Nguyen, H.B. Kim, E.D. Park, CO and CO2 Methanation over CeO2-Supported Cobalt Catalysts, Catalysts. 12 (2022). https://doi.org/10.3390/catal12020212.

[58] O. Tursunov, L. Kustov, Z. Tilyabaev, Methanol synthesis from the catalytic hydrogenation of CO2 over CuO–ZnO supported on aluminum and silicon oxides, J Taiwan Inst Chem Eng. 78 (2017) 416–422. https://doi.org/10.1016/j.jtice.2017.06.049.

[59] H. Ronduda, M. Zybert, W. Patkowski, A. Ostrowski, P. Jodłowski, D. Szymański, L. Kępiński, W. Raróg-Pilecka, A high performance barium-promoted cobalt catalyst supported on magnesium-lanthanum mixed oxide for ammonia synthesis, RSC Adv. 11 (2021) 14218–14228. https://doi.org/10.1039/d1ra01584b.

[60] C. Liu, X. Guo, Q. Guo, D. Mao, J. Yu, G. Lu, Methanol synthesis from CO2 hydrogenation over copper catalysts supported on MgO-modified TiO2, J Mol Catal A Chem. 425 (2016) 86–93. https://doi.org/10.1016/j.molcata.2016.09.032.

[61] T.A. Le, M.S. Kim, S.H. Lee, E.D. Park, CO and CO2 Methanation Over Supported Cobalt Catalysts, Top Catal. 60 (2017) 714–720. https://doi.org/10.1007/s11244-017-0788-y.

[62] N.D. Subramanian, G. Balaji, C.S.S.R. Kumar, J.J. Spivey, Development of cobalt-copper nanoparticles as catalysts for higher alcohol synthesis from syngas, Catal Today. 147 (2009) 100–106. https://doi.org/10.1016/j.cattod.2009.02.027.

[63] K. Sun, Z. Liu, S. Song, W. Liu, P. Wang, T. Zhang, Y. Xue, Y. Wang, Y. Tan, Effect of Hydroxyl Groups on CuCoMg Nanosheets for Ethanol and Higher Alcohol Synthesis from Syngas, Ind Eng Chem Res. 60 (2021) 2388–2399. https://doi.org/10.1021/acs.iecr.0c05204.

[64] S. Bai, Q. Shao, P. Wang, Q. Dai, X. Wang, X. Huang, Highly Active and Selective Hydrogenation of CO 2 to Ethanol by Ordered Pd − Cu Nanoparticles, (2017) 23–26. https://doi.org/10.1021/jacs.7b03101.

[65] J. Zheng, K. An, J. Wang, J. Li, Y. Liu, Direct synthesis of ethanol via CO2 hydrogenation over the Co/La-Ga-O composite oxide catalyst, Journal of Fuel Chemistry and Technology. 47 (2019) 697–708. https://doi.org/10.1016/S1872-5813(19)30031-3.

[66] K. Zhao, M. Calizzi, E. Moioli, M. Li, A. Borsay, L. Lombardo, R. Mutschler, W. Luo, A. Züttel, Unraveling and optimizing the metal-metal oxide synergistic effect in a highly active Cox(CoO)1–x catalyst for CO2 hydrogenation, Journal of Energy Chemistry. 53 (2020) 241–250. https://doi.org/10.1016/j.jechem.2020.05.025.

[67] Z. He, Q. Qian, Z. Zhang, Q. Meng, H. Zhou, Z. Jiang, B. Han, Synthesis of higher alcohols from CO2 hydrogenationovera PtRu/Fe2O3 catalyst under supercritical condition, Philosophical Transactions of the Royal Society A: Mathematical, Physical and Engineering Sciences.Trans.R.Soc.A. 373 (2015) 1–10. https://doi.org/http://dx.doi.org/10.1098/rsta.2015.0006.

[68] B. Liu, B. Ouyang, Y. Zhang, K. Lv, Q. Li, Y. Ding, J. Li, Effects of mesoporous structure and Pt promoter on the activity of Co-based catalysts in low-temperature CO2 hydrogenation for higher alcohol synthesis, J Catal. 366 (2018) 91–97. https://doi.org/10.1016/j.jcat.2018.07.019.

[69] Z. He, Q. Qian, J. Ma, Q. Meng, H. Zhou, J. Song, Z. Liu, B. Han, Water-Enhanced Synthesis of Higher Alcohols from CO2 Hydrogenation over a Pt/Co3O4 Catalyst under Milder Conditions, Angewandte Chemie - International Edition. 55 (2016) 737–741. https://doi.org/10.1002/anie.201507585.

[70] R. Chauvy, N. Meunier, D. Thomas, G. De Weireld, Selecting emerging CO2 utilization products for short- to mid-term deployment, Appl Energy. 236 (2019) 662–680. https://doi.org/10.1016/j.apenergy.2018.11.096.

[71] Y. He, S. Liu, W. Fu, J. Chen, Y. Zhai, X. Bi, J. Ren, R. Sun, Z. Tang, C. Mebrahtu, F. Zeng, Assessing the efficiency of CO2 hydrogenation for emission reduction: Simulating ethanol synthesis process as a case study, Chemical Engineering Research and Design. 195 (2023) 106–115. https://doi.org/10.1016/j.cherd.2023.05.043.

7. Appendix A (Supplementary Material)

Table S1. Reaction data for all presented catalysts and reaction conditions. All catalytic tests were conducted at 30 bar.

Catalyst	T_R [a] (ºC)	T [a] (ºC)	R [b]	GHSV [c]	X_{CO2} (%)	Selectivity (%)						Yield (mmol.g_{cat}^{-1}.h^{-1})			
						CO	CH_4	HCs (C_{2-5})	ROH			HCs (C_{2-5})	ROH		
									C_1	C_2	C_{3+}		C_1	C_2	C_{3+}
$Cu_{2.6}AlO_x$	250	250	3:1	14200	8.8	78.8	0	0	21	0	0	0	2.78	0	0
$Co_{1.3}Cu_{1.3}AlO_x$	250	250	3:1	14200	14.6	0	68.9	19.6	1.6	5.4	4.5	1.77	0.34	0.59	0.32
$Co_{1.8}Cu_{0.9}AlO_x$	250	250	3:1	14200	11.3	0	52.5	31.0	0.4	8.4	7.7	2.12	0.07	0.71	0.43
$Co_{2.6}AlO_x$	250	250	3:1	14200	5.3	0	59	18.8	7.2	6.7	8.3	0.63	0.56	0.26	0.21
$Co_{2.6}AlO_x$	300	250	3:1	14200	6.9	0	53.4	28.9	2.0	6.3	9.4	1.11	0.2	0.32	0.33
$Co_{2.6}AlO_x$	400	250	3:1	14200	9.8	0	44.1	35.4	0.3	10.6	9.6	2.03	0.04	0.77	0.46
$Co_{2.6}AlO_x$	500	250	3:1	14200	51.8	0	90.1	5.6	0.0	2.1	2.2	1.74	0	0.79	0.57
$Co_{1.8}Cu_{0.9}AlO_x$	300	250	3:1	14200	12.6	0	45.1	30.5	0.7	10.6	13.1	2.18	0.13	0.97	0.79
$Co_{1.8}Cu_{0.9}AlO_x$	400	250	3:1	14200	17.1	0	39.5	31.3	0.7	12.0	16.5	3	0.18	1.55	1.35
$Co_{1.8}Cu_{0.9}AlO_x$	500	250	3:1	14200	12.0	0	47.8	34.9	0.6	8.6	8.1	2.35	0.11	0.78	0.51
$Co_{1.8}Cu_{0.9}AlO_x$	400	200	3:1	14200	7.1	0	53.4	21.8	0.4	12.3	12.1	0.95	0.04	0.65	0.43
$Co_{1.8}Cu_{0.9}AlO_x$	400	300	3:1	14200	30.1	9.4	45	31.2	3.4	4.1	6.9	4.84	1.52	0.91	1.03
$Co_{2.6}AlO_x$	400	200	3:1	14200	3.0	0	49	19.3	2.3	16.5	12.9	0.34	0.1	0.37	0.19
$Co_{2.6}AlO_x$	400	300	3:1	14200	19.5	14.2	40.6	28.7	5.1	5.5	5.9	3.25	1.49	0.81	0.6
$Co_{1.8}Cu_{0.9}AlO_x$	400	250	3:1	10625	24.4	0	28.4	31.6	0.3	17.3	22.4	3.24	0.08	2.39	2.15
$Co_{1.8}Cu_{0.9}AlO_x$	400	250	3:2	14200	12.2	0	22.5	32.3	0.4	20.8	24.0	3.54	0.12	3.08	2.46

[a] T_R: reduction temperature; and T: reaction temperature.
[b] R: H_2/CO_2 ratio.
[c] GHSV expressed in mL.g_{cat}^{-1}.h^{-1}.

Table S2. Hydrocarbons yield distribution for all presented catalysts and reaction conditions. All catalytic tests were conducted at 30 bar.

Catalyst	T_R [a] (ºC)	T [a] (ºC)	R [b]	GHSV [c]	X_{CO2} (%)	HCs Yield (mmol.g_{cat}^{-1}.h^{-1}) [d]							
						C2=	C2	C3=	C3	C4=	C4	C5=	C5
$Cu_{2.6}AlO_x$	250	250	3:1	14200	8.8	0	0	0	0	0	0	0	0
$Co_{1.3}Cu_{1.3}AlO_x$	250	250	3:1	14200	14.6	0.00	1.06	0.01	0.70	0	0	0	0
$Co_{1.8}Cu_{0.9}AlO_x$	250	250	3:1	14200	11.3	0.02	1.14	0.21	0.76	0	0	0	0
$Co_{2.6}AlO_x$	250	250	3:1	14200	5.3	0	0.42	0	0.21	0	0	0	0
$Co_{2.6}AlO_x$	300	250	3:1	14200	6.9	0.1	0.43	0.27	0.18	0.07	0.02	0.01	0.03
$Co_{2.6}AlO_x$	400	250	3:1	14200	9.8	0	1.02	0.21	0.72	0.04	0.04	0	0
$Co_{2.6}AlO_x$	500	250	3:1	14200	51.8	0.03	1.06	0.15	0.37	0.06	0.02	0.02	0.03
$Co_{1.8}Cu_{0.9}AlO_x$	300	250	3:1	14200	12.6	0.03	1.09	0.31	0.64	0.07	0.04	0	0
$Co_{1.8}Cu_{0.9}AlO_x$	400	250	3:1	14200	17.1	0.13	1.3	0.56	0.73	0.19	0.07	0.01	0.01
$Co_{1.8}Cu_{0.9}AlO_x$	500	250	3:1	14200	12.0	0.12	1	0.36	0.63	0.09	0.1	0.02	0.03
$Co_{1.8}Cu_{0.9}AlO_x$	400	200	3:1	14200	7.1	0.03	0.51	0.04	0.33	0.01	0.03	0	0
$Co_{1.8}Cu_{0.9}AlO_x$	400	300	3:1	14200	30.1	0.45	1.68	0.95	0.91	0.33	0.28	0.06	0.18
$Co_{2.6}AlO_x$	400	200	3:1	14200	3.0	0	0.17	0	0.15	0	0.02	0	0
$Co_{2.6}AlO_x$	400	300	3:1	14200	19.5	0.52	1.19	0.36	0.89	0.15	0.12	0.01	0.01
$Co_{1.8}Cu_{0.9}AlO_x$	400	250	3:1	10625	24.4	0.17	1.16	0.83	0.59	0.25	0.17	0.03	0.04
$Co_{1.8}Cu_{0.9}AlO_x$	400	250	3:2	14200	12.2	0.29	1.29	0.85	0.63	0.29	0.09	0.04	0.06

[a] T_R: reduction temperature; and T: reaction temperature.
[b] R: H_2/CO_2 ratio.
[c] GHSV expressed in mL.g_{cat}^{-1}.h^{-1}.
[d] HCs are separated by the number of carbons and whether they are paraffins (C2, C3) or olefins (C2=, C3=).